CHARACTERIZATION OF ALUMINUM CORROSION PRECIPITATES IN SUPPORT OF GSI-191 HEAD LOSS TESTING

A Thesis

by

CHRISTOPHER TODD FULLERTON

Submitted to the Office of Graduate and Professional Studies of
Texas A&M University
in partial fulfillment of the requirements for the degree of

MASTER OF SCIENCE

Chair of Committee,	Yassin A. Hassan
Co-Chair of Committee,	Rodolfo Vaghetto
Committee Member,	Maria D. King
Head of Department,	Yassin A. Hassan

August 2017

Major Subject: Nuclear Engineering

ABSTRACT

In the event that a nuclear core cooling pipe ruptures, a loss of coolant accident (LOCA) scenario begins. Precipitates from dissolved ions can form and cause the emergency backup pumps to fail. Two aluminum products, an aluminum oxyhydroxide (AlOOH) and aluminum oxide solid are expected to have the greatest impact on debris bed formation. The objective of this experimental study was to classify these compounds by size, structure, and behavioral characteristics, and compare them to a benchtop salt generated precipitate made with aluminum nitrate nonahydrate. The source of the aluminum ions varies by plant, but they typically originate from corrosion of structures in the reactor containment environment. Characterizing the aluminum corrosion product is necessary to determine if an aluminum surrogate salt precipitate product can be substituted in the Nuclear Regulatory Commission's (NRC) generic safety issue-191 (GSI-191) head loss testing to simplify testing procedures. If the surrogate salt product is comparable to the alloy corrosion product, it will simplify the task of studying sump strainer debris bed formation in future testing.

The representative post LOCA coolant solution for this experimental study was created at varying pH's representative of containment chemistry. Aluminum samples were corroded at 85℃ ± 2℃ until the solubility limit was reached. The aluminum source was removed and the solution was cooled to 25℃ at three different cooling rates. The resulting solution was analyzed for turbidity, particle size, TEM, XRD, and settling characteristics. These results are compared to an aluminum nitrate nonahydrate surrogate

salt precipitate prepared according to industry standards and regulations. The characterization of the precipitates proved to be dependent on corrosion pH, aluminum ion concentration, and cooling rate. The cooling rate dynamics indicate a higher probability of large precipitate formation during slow cooling rates and smaller particle formation during rapid cooling rates. The quantity of particles generated was assessed with solution turbidity. The solutions with higher concentrations of aluminum ions resulted in higher solution turbidity. The AlOOH precipitates from the $Al(NO_3)_3 \bullet 9H_2O$ salt solution were determined to be a suitable substitute for further head loss testing in the chemical GSI-191 project.

DEDICATION

A thesis dedicated to my wonderful and supportive parents, siblings, and friends alike. These people helped shape me into who I am today and have always been there to support and help guide me through this path of life.

"Only those who will risk going too far can possibly find out how far they can go"

-T.S. Eliot

"Science is organized knowledge. Wisdom is organized life"

-Immanuel Kant

ACKNOWLEDGEMENTS

I would like to thank my committee chair, Dr. Yassin A. Hassan, as well as Dr. Rodolfo Vaghetto, Dr. Saya Lee and Dr. Maria King for their guidance and support throughout the course of this research. A special thanks goes out to Dr. Jeanette Leavitt for insight and direction necessary in the completion of this thesis.

Thanks also go out to my friends and colleagues and the department faculty and staff for making my time at Texas A&M University a great and truly memorable experience that I will never forget.

Finally, thanks to my mother, Mary Fullerton, my father Paul Fullerton, and my brothers and sister Jeff, Jan, and Allie for their encouragement and support.

CONTRIBUTORS AND FUNDING SOURCES

Faculty committee recognition

This work was supervised by my thesis committee consisting of Dr. Yassin A. Hassan as chair, Dr. Rodolfo Vaghetto as co-chair, and Dr. Maria King as committee member.

Student collaborator contributions

The data analyzed for the IPC-MS section of this study was provided by Vijay Ravisankar and Dr. Ugaz in the Texas A&M Chemical Engineering Department. All other work conducted for the thesis was completed by the student independently.

Funding sources

This graduate study was supported by a fellowship from Texas A&M University and in part by funding and collaboration from Palisades Nuclear Generating Station.

NOMENCLATURE

BWR	Boiling Water Reactor
DI	De-Ionized
DLS	Dynamic Light Scattering
ECCS	Emergency Core Cooling System
GSI-191	Generic Safety Issue-191
ICP-MS	Inductively Coupled Mass Spectrometry
IC	Intermediate Cooled
LOCA	Loss of Coolant Accident
NaTB	Sodium Tetraborate$_{(s)}$
NRC	Nuclear Regulatory Commission
NTU	Nephelometric Turbidity Unit
PDI	Poly-Dispersity Index
PWR	Pressurized Water Reactor
RC	Rapid Cooled
RHR	Residual Heat Removal (pumps)
RO	Reverse Osmosis
SC	Slow Cooled
TDS	Total Dissolved Solids
TEM	Transmission Electron Microscope
WCAP	Westinghouse Commercial Atomic Power
XRD	X-Ray Diffraction

TABLE OF CONTENTS

Page

Page

LIST OF FIGURES

Page

Page

Page

Page

LIST OF TABLES

Page

INTRODUCTION

Background

GSI-191 was created to resolve outstanding issues of debris accumulation on reactor sump strainer screens in pressurized water reactors (PWR's) and boiling water reactors (BWR's) plants that was not addressed in NRCB 93-02. Ongoing efforts have been made by the nuclear industry and the Nuclear Regulatory Commission (NRC) to address post LOCA PWR sump strainer issues since 1997 (Leeds, E., 2010). In the 1990's through the 2000's, the United States NRC required many existing plants to evaluate possible sump strainer clogging. These problems can arise due to various debris and chemical precipitate products that may form and accumulate immediately following a LOCA event. Initial awareness of the issue arose after a LOCA occurrence at the Barseback nuclear generating station in Sweden occurred (Lee, J., 2011; Sandrine, R., 2008). The BWR plant suffered a failure of the emergency core cooling system (ECCS) due to a sump strainer clogging (Lahti, E., 2014). In the event that the pumps are unable to circulate coolant, it can lead to additional problems with the ECCS resulting in possible core and fuel damage (Bahn, C., 2013).

On July 28, 1992, just outside Copenhagen Sweden, an unplanned event occurred in the Barseback Unit 2 BWR containment facility. Two ECCS pump strainers became partially blocked after high pressure steam and water was released at 3100kPA and caused debris transport to the strainer region. The immediate cause of the clog was the result of mineral wool insulation that had been dislodged at the time of the rupture. The

operators of the plant were able to reverse the flow direction of the ECCS loop and clear the strainers of debris, but it was clear that further risk analysis would need to be completed to prove these systems are effective and reliable (NRCB 96-03).

Motivation was escalated after two additional events occurred in 1993 at the Ohio Perry Nuclear Power Plant. The first event caused the residual heat removal pumps (RHR's) to clog. The second event involved the same RHR pumps, but this time a large influx of glass particulate in the form of fibers from insulation collected on the pump strainers. These fibers increased the filtration ability of the strainers allowing more debris to sit on the strainer resulting in further head loss. The debris included precipitates from corrosion products that were generated in the containment pool chemistry (NRCB 96-03). According to Section 50.46, Title 10 of the Code of Federal Regulations, any nuclear power plant that is currently operational is required to have an ECCS that can provide both short term as well as long term cooling capabilities to the core. Addressing this issue was initially classified under the Unresolved Safety Issue A-43, which specifically analyzed fiber transport and settling characteristics. With the introduction of GSI-191, additional parameters to be analyzed included LOCA coolant chemistry and possible precipitate formation that may occur in this environment (NRCB 93-02).

Initially, a blanket study was performed to evaluate risk analysis for all currently operating PWR and BWR plants in the United States. This was problematic due to the vast differences in design parameters for each plant including size, layout, coolant chemistry, strainer configurations and locations as well as insulation types used

in each plant. To resolve the outstanding issues categorized under GSI-191, the US-NRC created the PWR Sump Performance Task Force. This task force was faced with the challenge of interfacing with individual plants and the US-NRC to create and validate safety concerns for each plant (Borchardt, R. W., 2012). To maintain licensing, the US-NRC required that each plant perform a risk analysis study to determine specific risk characteristics for each reactor layout (NEI 04-07).

Scope of Study

During a LOCA in a PWR or BWR, a substantial quantity of debris can be released into the containment facility surrounding the reactor core. The debris generated includes Nukon fiberglass insulation, dirt, paint, and a significant quantity of ions from varying sources (Jeong-lk., et al, 2011). The debris along with other LOCA related effects such as temperature, pH change and other chemical effects can cause head loss across the sump strainer screens which can result in overheating of the core and fuel elements due to failure of the ECCS. The focus of this study is to specifically investigate the conditions related to aluminum chemical precipitate products formed immediately after a LOCA scenario as well as during reactor cool down post-accident. These chemical precipitates then will be analyzed and compared to an aluminum salt substitute precipitate to validate existing risk assessment studies that have already been conducted or are in progress (Fullerton, C., 2015 (1); Fullerton, C., 2015 (2); Fullerton, C., 2015 (3)).

Specifics of Study

The approach used was developed to specifically study the chemical precipitate effects within typical PWR containment environments. Specific materials were analyzed for leaching characteristics including aluminum alloys. According to the GSI-191 issue, the materials of highest concern are: calcium, aluminum and silicon (Klasky, M., 2006). Due to the specifics of the PWR plants studied, the calcium leaching issue was ignored since the buffer typically used is sodium tetraborate (NaTB) and not tri-sodium phosphate. Focusing specifically on NaTB as the buffer allows for the assumption that $Ca_3(PO_4)_2$ is not likely to form in the post LOCA solution (Fullerton, C., 2015). Since the exact concentration of ions released into containment after a cooling pipe rupture is a function of break size and location of the break, the worst-case scenario precipitate generation was used as a conservative model in this study. Table 1 details a typical PWR aluminum source inventory that was used for modeling.

Table 1 - Detailed worst-case aluminum inventory at a typical PWR generating plant

Submerged or Destroyed (Both sides wetted)			
Aluminum Source	**Thickness (in)**	**Surface Area (ft^2)**	**Weight (lb_m)**
Paint	3.94E-04	56297	156
Reactor Vessel Reflective Metal Insulation	6.50E-04	30344	139
RMI (in Bioshield Penetration)	1.00E-03	40660	286
Mineral Wool	2.50E-03	3132	55
Service Insulation	1.60E-02	4766	535
Large Break Mineral Wool (corrugated Al)	3.20E-02	1578	355
Reactor Vessel Insulation supports	1.25E-01	458	361
Reactor Cavity Insulation Supports	2.50E-01	264	440
Submerged Total		**137499**	**2327**
Sprayed (One side wetted)			
Aluminum Source	**Thickness (in)**	**Surface Area (ft^2)**	**Weight (lb_m)**
Pipe Covering	1.60E-02	12420	2809
Pressurizer Jacket	3.20E-02	0	0
Light Fixtures	6.25E-02	700	600
Total Sprayed		**13120**	**3409**

Effects of Aluminum Corrosion Products

After a LOCA scenario and during the cooldown phase, one of the substantial products formed in solution is an aluminum oxyhydroxide (AlOOH) and aluminum oxide solid Al_2O_3 (Bahn, 2013). The source of the aluminum ions varies by plant, but typically originates from corrosion of scaffolding, fans, blades, hubs, and valves. (Ghosh et al., 2007) The aluminum precipitate can then accumulate with fiberglass and other

LOCA debris on sump strainers and can cause additional head loss across strainer screens (Lahti, E., 2014).

The effect of accumulation of both fiberglass and aluminum precipitate products at the sump screen can result in head loss of up to two orders of magnitude larger than with fiberglass alone (Bahn, C., 2013). It is therefore necessary to characterize the aluminum corrosion product created to determine if an aluminum surrogate salt precipitate can be substituted for GSI-191 testing without introducing substantial errors. It has been remarked that preparation of a surrogate salt precipitate with the use of an aluminum salt can result in highly random structures (Klasky, M., 2006).

Tests were performed according to prototypical BWR and PWR LOCA conditions. The pH was varied to three discreet values of 7.2, 7.5 and 8.2. The lower pH spectrum was chosen to represent typical containment conditions needed to ensure the release of volatile radioactive iodine was minimized and the upper values represent a worst-case scenario necessary to produce enough aluminum ions in solution to generate an observable precipitate product. (Lane et al., 2008). If the precipitate products are sufficiently large, or demonstrate characteristics that are likely to result in deposition on the sump strainer screens, it can cause additional safety equipment to fail due to a loss of coolant to the core (Sandrine, R., 2008).

The sump strainer screens are designed to catch debris inside the containment facility to prevent it from causing subsequent damage to the ECCS. However, a large buildup on the screens can also cause the ECCS systems to fail if they are unable to

transport water from the containment region (Bahn et al., 2013). As the sump screens clog, the head across the sump pump membrane decreases presenting a possible scenario where the core could become improperly cooled resulting in a possible high risk accident scenario (Bahn et al., 2013).

MATERIALS AND METHODS

Overview

This study focused specifically on aluminum corrosion products that were generated from a representative aluminum source used in reactor containment buildings. A representative LOCA coolant solution containing boric acid (H_3BO_3) along with a buffer solution of NaTB ($Na_2B_4O_7 \bullet 10H_2O$) to stabilize pH at the desired values was used. Table 2 lists the chemical concentrations used to represent standard and worst-case scenario pH values for the post LOCA water chemistry. The solution was created in a 340L stainless steel tank and heated to 85 °C ± 2°C before the aluminum coupons were added to corrode. The solution was permitted to circulate and corrode the aluminum until the saturation point was reached. (Vujičić, V., 1985). After corrosion, the foil was removed and aqueous samples were taken for inductively coupled plasma mass spectrometry (ICP-MS) to determine exact aluminum concentrations. Six additional 1-L samples were also taken from the tank immediately following corrosion and cooled via two different rates. Three of the six samples were placed in an ice bath for rapid cooling data and the other three were placed in an oven that was manually adjusted to simulate a slower cooling rate. The tank was also permitted to naturally cool without circulation representing an intermediate cooling rate sample.

Table 2 - Simulated post LOCA coolant chemistry conditions

Test pH	**Boric Acid (g/L)**	**NaTB (g/L)**
7.2	14.60	2.86
7.5	11.51	3.27
8.2	4.68	3.27

The samples taken were compared for precipitate composition via turbidity measurements, particle size analysis, TEM, and EDS. Further analysis was performed on the aluminum corrosion products to provide insight on precipitate characteristics including size, morphology, and quantity (Zhou, Q., 2012). The exact final concentration of aluminum was not standardized for all tests, but was measured and recorded for each test. The objective was to reach a concentration that approached or reached the saturation limit at the corrosion temperature and pH in the allotted test duration (Vujičić, V., 1985).

The tests were conducted using stainless steel corrosion tanks pictured in Figure 1. Aluminum ions were produced in the tanks from the corrosion of the aluminum alloy. The solution was cooled via differing rates and the precipitate generation was analyzed. Precipitation of the varying aluminum compounds was induced by cooling the solution to room temperature (25° C +/- 3°C).

Currently little research has been conducted to analyze the impact of cooling rates and pH effects on the formation of aluminum precipitates in post LOCA water chemistry (Kim, S.J., Howe, K. J., 2013).

Figure 1 - TAMU corrosion tank facility without insulation (left) and with insulation (right).

Figure 2 shows the schematic for the corrosion tank. The flow path during circulation through the corrosion tank is from the pump intake labeled as V-C1-1, where the solution then flows up through open valve V-C1-3, through the temperature controlled immersion heaters (H-C1-1 and H-C1-2), and back into the tank through V-C1-6.

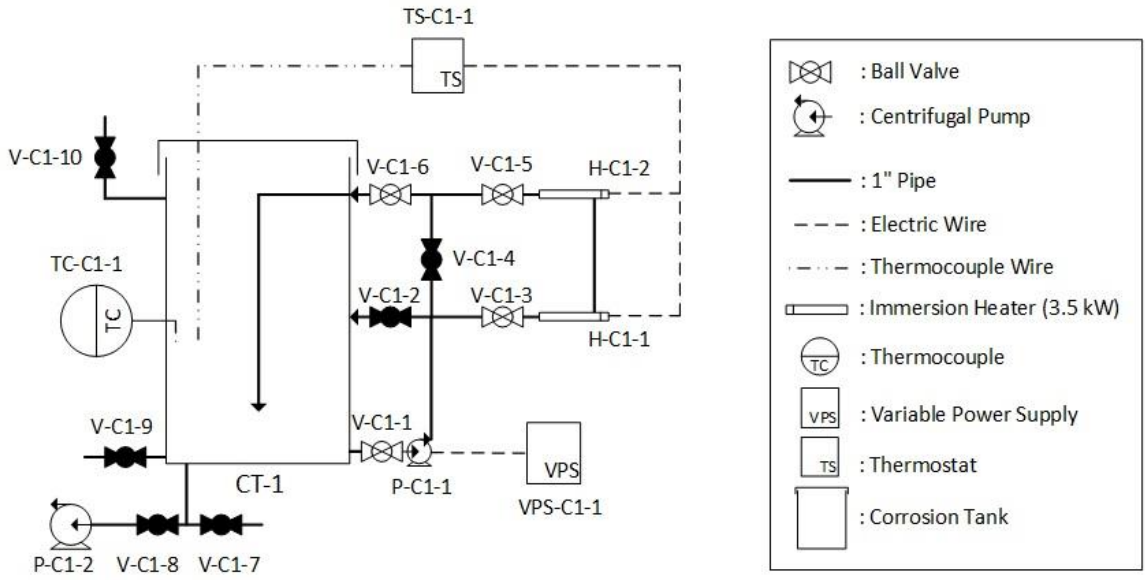

Figure 2 - Corrosion tank schematic for Al precipitate generation.

Materials

The boric acid and NaTB were obtained from certified vendors that supply nuclear grade reagents. The 1145 alloy aluminum foil used was 1.5 mils thick and representative of the aluminum sources commonly found in current PWR's. Figure 3 and Figure 4 show generic aluminum preparation pictures representative of all 3000 test series experiments performed. The outer layer of the bulk aluminum roll was removed and discarded prior to each test to prevent any unwanted contamination that may have adhered to the outer foil surface. The aluminum was then cut into three approximately equal massed sections. They were rinsed with reverse osmosis (RO) water to remove any contaminants before being loosely rolled into three cylindrical sections.

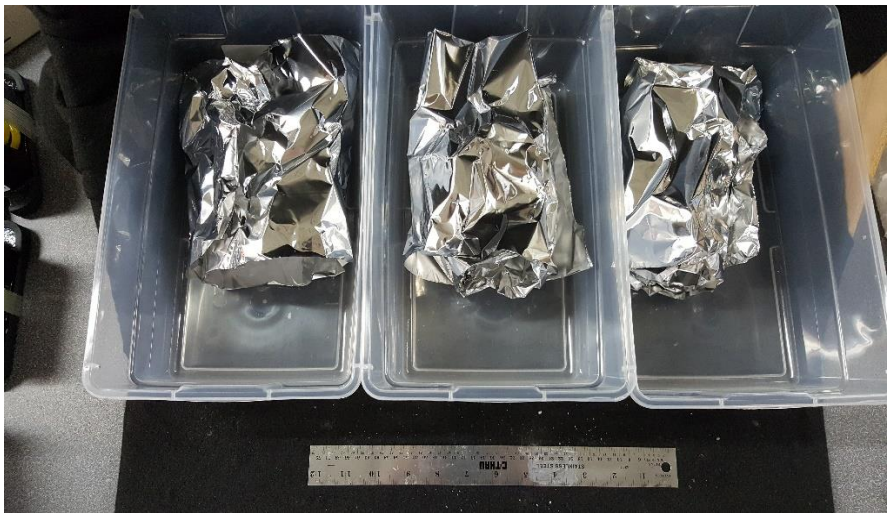

Figure 3 - Generic aluminum preparation for 3000 series tests.

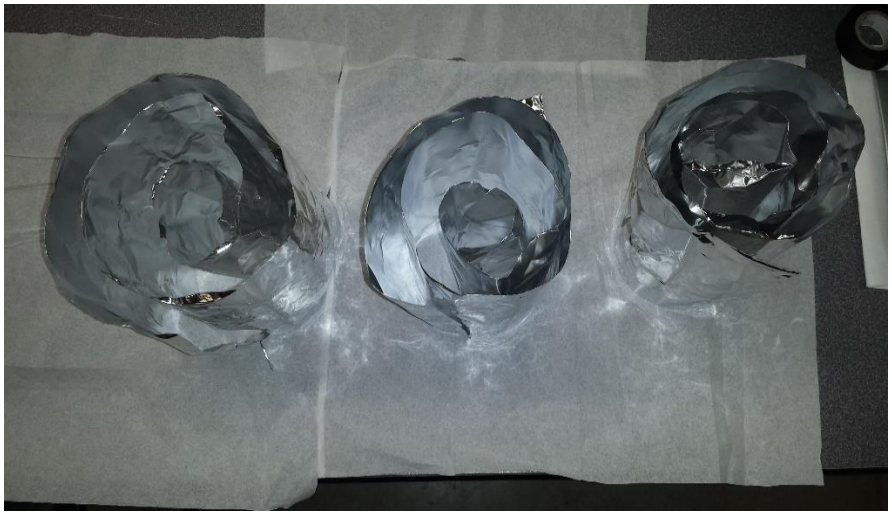

Figure 4 - Representative foil roll geometry for 3000 series tests.

Instrumentation

All instruments were calibrated at minimum according to manufacturer recommendations. The solution pH was verified prior to each test within a ± 0.1 interval for each test target value before testing commenced. All water used was prepared with a RO system as outlined in the Water Preparation section. Electrical conductivity of the water was maintained below 15 µS/cm prior to chemical addition. All test samples were taken in polypropylene containers and were stored at room temperature after testing.

Water Preparation

All water used for corrosion experiments was thoroughly filtered and deionized through a RO system prior to use. The system used for filtration was a Flexeon CT-7000 Commercial Reverse Osmosis System, seen in Figure 5. The system was coupled with four Axeon HF5-4040 2500 GPD RO membrane elements. The water was pre-treated prior to the RO system with a coupled filtration system consisting of two activated carbon filters, one 25-micron polypropylene filter, and one 0.1-micron polypropylene sediment filter. The filtered water was tested with a PCS Testr 35, shown in Figure 5, for electrical conductivity prior to use.

Figure 5 - Flexeon CT-7000 commercial reverse osmosis system and coupled pre-treatment filters (left), PCS Testr 35 EC/pH/TDS meter (right).

Test Preparation

Tank Preparation and Cleaning

Prior to testing, the stainless-steel corrosion tanks were thoroughly cleaned. This process involved a thorough washing of the tank with Citranox®, an aqueous acidic cleaning detergent, to dissolve any residual ions that may have been left adhered to tank surfaces from previous testing. The tanks were then thoroughly rinsed out until the electrical conductivity and TDS standards were met. The tanks were then thoroughly rinsed out once more and filled with RO water. The filled tanks were then checked for electrical conductivity and pH again.

Solution Preparation and Test Commencement

The clean corrosion tank was filled with 190L of RO water. Boric acid and NaTB were then added to dissolve and the pH was verified to be within a ±0.1 interval for the specified test. The immersion heaters in the recirculation loop were turned on and aluminum coupons were added once the tank reached the elevated target temperature of 85C ±2 ℃. The temperature was turned down to 80℃ for the duration of the test. After running for 4 hours, the recirculation pump was turned off, the aluminum removed from solution, and the tank insulation was removed to facilitate cooling. A sample was taken at the end of the 4-hour mark for ICP-MS and was acidified with HNO_3.

To analyze the effects of cooling rate on precipitate generation, three samples were taken from the tank immediately after corrosion and placed directly into an ice bath. The temperature of these rapid cooled (RC) samples was monitored until they reached room temperature (25°C), after which, they were removed from the bath. Three additional samples were taken and placed into an oven that was set between 50 °C and 60 °C for 24 hours and was then turned off to generate slow cooled (SC) samples. The temperatures of all samples were monitored during the cooling process. After approximately 48 hours, the tank had cooled to room temperature and a sample was taken for the intermediate cooled (IC) sample. Prior to tank sampling, the pump was turned on briefly to ensure samples taken from the tank were homogeneous. The size and turbidity of all samples were monitored over the next month to see if any significant changes occurred which would indicate an unstable precipitate product may have formed

or flocculation or conglomeration may have occurred. Possible negative effects of mixing with the pump were verified to be negligible by taking a sample prior to and after mixing with the pump to ensure the pump turbine did not break up any flocculated particles. These samples were later compared for particle size via DLS

ICP-MS Analysis

A sample was taken from the tank at the end of each test and acidified in a 1:250 volumetric ratio of HNO_3[1] to precipitate solution. This ensured that any aluminum in solution would not precipitate out prior to ICP-MS analysis. The instrument used to measure the samples was a Perkin Elmer NexIon 300D ICP Coupled Mass Spectrometer. The samples required dilution to be measured with the 300D ICP-MS accurately since our concentration range was above the upper detection limit of the instrument. This dilution was carried out based on preliminary testing which provided an approximate expected concentration for each solution. A calibration curve was created in the expected aluminum concentration range and compared to all samples run to determine dissolved aluminum ion concentration of the sample.

An aluminum standard[2] was used to prepare the calibration curve for the ICP-MS analysis. The standards were prepared within the range of 25- 125 ppb by diluting the standard first with a spike solution identical to the original corrosion solution for each test and then with additional DI water. The spike solution was confirmed to have the same pH as the original corrosion solution for each test before being used in the ICP-MS analysis. The sample obtained from the corrosion test was assumed to have an

[1] ACS reagent grade (70%) nitric acid CAS#7697-37-2
[2] aluminum standard 61935, FLUKA for ICP (1000mg/L)

approximate concentration of 50-100ppm depending on corrosion pH and was then diluted accordingly with RO water so it fell within the measurement range (2-200ppb) for the ICP-MS instrument.

Turbidity Analysis

Samples taken during testing were subject to initial turbidity measurements as well as additional measurements over the following 30 days. If a significant change in turbidity was noted, additional size measurements could be run to confirm whether or not there was a change from the initial measured particle size. A HACH 2100Q portable turbidimeter displayed in Figure 6 was calibrated with 4 NIST traceable formazin standards before measuring any samples. The standards used were HACH 10, 20, 100 and 800 NTU primary standards.

Figure 6 - HACH 2100Q portable turbidimeter.

Particle Size Analysis

The Malvern Zen 3600 DLS was calibrated with Duke Scientific 3060A and Thermoscientific (3100A) NIST traceable 60nm 100nm standards in a 1:30 dilution of RO water. The size specifications of the standards are listed in Table 3. The instrument material refractive index for the standards was set to 1.77, material absorption to 0.10 in a deionized DI water dispersant. The material refractive index and absorption were also set to 1.77 and 0.10 respectively for the alumina samples. The measurement duration for standards and samples was set at 80 seconds. Table 4 shows the full settings used for sample analysis.

Table 3 - Polystyrene microsphere standards specifications.

Standard	**Catalog Number**	**Description**	**Mean Diameter**	**%RSD** $(\sigma/\mu)*100$
Duke Scientific 60nm Microsphere	3060A	Polymer microspheres in water	60nm (+/- 4nm)	17%
Thermo Scientific 100nm Nanosphere	3100A	Polymer microspheres in water	100nm (+/- 3nm)	7.8%

Table 4 - Zen 3600 sample settings for aluminum measurements.

Setting	**Value**
Material Refractive Index	1.77
Material Absorption	0.010
Dispersant Type	DI Water
Dispersant Refractive Index	1.33
Viscosity	0.8872
Temperature	(25°C +/- 3°C)
Measurement Duration	80 Seconds

TEM Analysis

The samples that were analyzed via transmission electron microscopy (TEM) were sonicated for 10 min and dropped on copper grids (Tedpella, Prod # 01881-F). The grids were dried at room temperature for 30 minutes before the measurements. Elemental analysis was performed on a TECNAI F20 Super-Twin transmission electron microscope (TEM) fitted with a Schottky field emission gun, a 2k x 2k Gatan CCD camera, and an EDAX instruments ultrathin window energy dispersive X-ray spectroscopy (EDX) detector. Different areas of interest were imaged by TEM and component elements of selected spots were analyzed by EDX. Both TEM images and EDX spectra were collected at a 200 kV accelerating voltage.

WCAP Precipitate

WCAP Summary of Methods

The WCAP 16530 NP alumina surrogate precipitate generation was performed on a bench scale setup to gather and analyze AlOOH precipitate products generated during a drop in pH. Aqueous solutions of $Al(NO_3)_3 \bullet 9H_2O$ ranging from 13.1g/L to 68.8g/L were developed and prepared in benchtop experiments. These salt surrogate solutions were then precipitated with the addition of NaOH and the precipitates were collected for further analysis.

WCAP Test Methods

Precipitation of the AlOOH was completed with the introduction of NaOH, but actually initiated prior to this with the introduction of the aluminum nitrate nonahydrate into the pH 7.2 borated solution (Fullerton, C., 2015 (4)). Test conditions for this test are summarized in Table 5. The pH, temperature, and mixing rate conditions are listed below. Figure 7 shows the benchtop setup used to prepare the WCAP precipitate product which consisted of a 2L beaker, stir bar and stir plate.

Table 5 - Materials used in 1100 series WCAP test.

Material	**Target**	**Actual**
Water (RO H_2O)	1.0 L	1.0 L
Boric acid (dry)	14.604 g	14.604 g
Sodium Tetraborate (dry)	2.857 g	2.857 g
Aluminum Nitrate Nonahydrate	1.088 g	1.087 g
NaOH	0.348 g	0.343 g

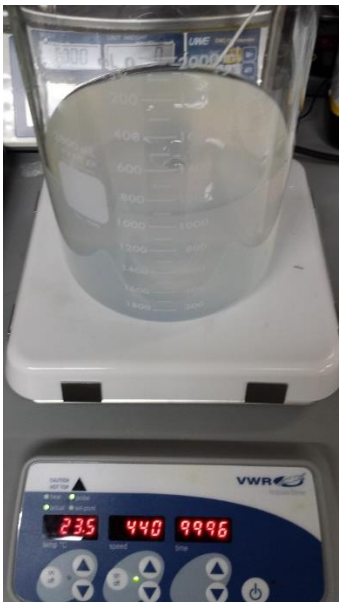

Figure 7 - WCAP aluminum precipitate generation setup.

Solution pH

The pH of the WCAP benchtop solution was made according to the concentrations listed for the pH 7.2 solution and was confirmed to be within +/- 0.1 of the 7.2 target value. The pH was checked and recorded before the start of the test, again once the boric acid and NaTB were dissolved, then once more after the $Al(NO_3)_3 \bullet 9H_2O$ was dissolved and finally once more after the NaOH was added.

Temperature

The temperature profile for this test was maintained at room temperature (25 +/- 2 °C) throughout the entirety of the test.

Turbidity Measurements

A HACH 2100Q portable turbidimeter was used to perform the turbidity measurements. The instrument was calibrated with 4 NIST traceable formazin standards before measuring a sample's turbidity. The standards used were 10, 20, 100 and 800 NTU primary standards to enable a repeatable and accurate calibration. The samples were visually inspected prior to measurement to ensure that no air bubbles, scratches or contaminants were present on the glass vial before reading.

Particle Size

A Malvern ZEN 3600 DLS was used to measure particle size of the aluminum precipitate formed during the experiment. The Malvern ZEN 3600 was calibrated with two NIST traceable standards, a 60nm and 100nm diameter polystyrene microsphere solution. The standards were created in a 1:30 dilution ratio for a total volume of 1.5mL before being analyzed in the machine. The standards were run in a 10x10x45mm polystyrene cuvette.

The samples taken after the precipitation reaction completed were analyzed undiluted using dynamic light scattering (DLS) in standard disposable polystyrene cuvettes to ensure no contamination. The solution was gently inverted 2-3 times before being drawn up into a pipette and then placed into the cuvette. This ensured that the sample was homogeneously mixed, minimizing any air bubbles that may have formed with aggressive agitation. The measurement performed by the DLS consisted of three

runs with 15 measurements per run. The signal was averaged for the final reading. The results for this analysis are reported in volume percent unless otherwise noted.

RESULTS

Cooling Rates

A summary of the cooling rates for pH 7.2, 7.5 and 8.2 tests for the RC, IC, and SC samples are presented in Table 6. The full cooling rate profiles for all tests are visible in Figure 8 to Figure 15.

Table 6 - Cooling rate summary for corrosion tests.

	Cooling Rate (℃ / hr) **pH: 7.2, 7.5, 8.2**	**Total Cooling Time (hr)** **pH: 7.2, 7.5, 8.2**
Rapid Cooled	144, 210, 223	0.33, 0.23, 0.27
Intermediate Cooled	2.2, 2.4, 2.0	25, 25, 28
Slow Cooled	1.4, 1.8, 1.8	33, 31, 32

3101/3201- Cooling Profile

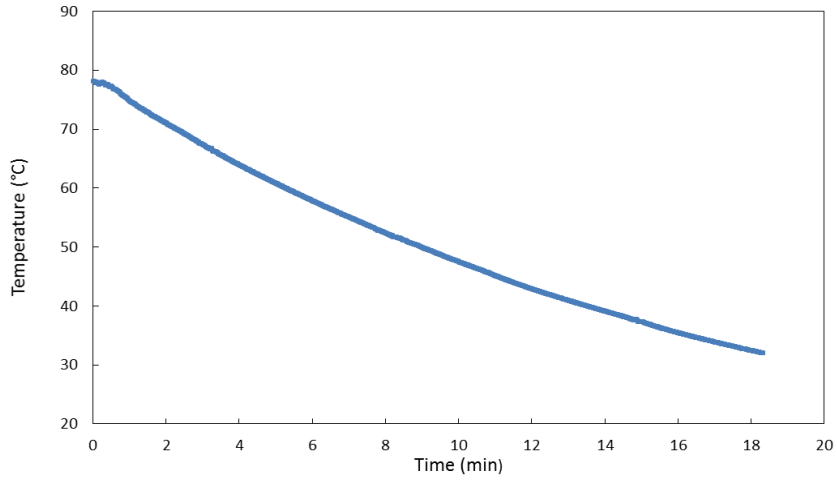

Figure 8 - Average cooling rate for 3 RC samples from 80 ℃ to room temperature (25 ℃) for pH 7.2 test.

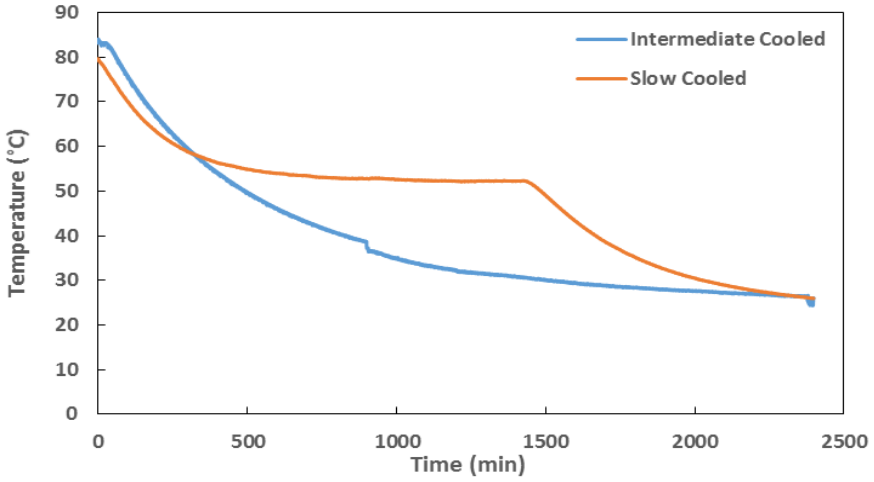

Figure 9 - IC rate and average cooling rate trend for 3 SC samples from 80 ℃ to room temperature (25 ℃) for pH 7.2 test. Oven was turned from 50°C to off at 1500 min.

3102/3202- Cooling Profile

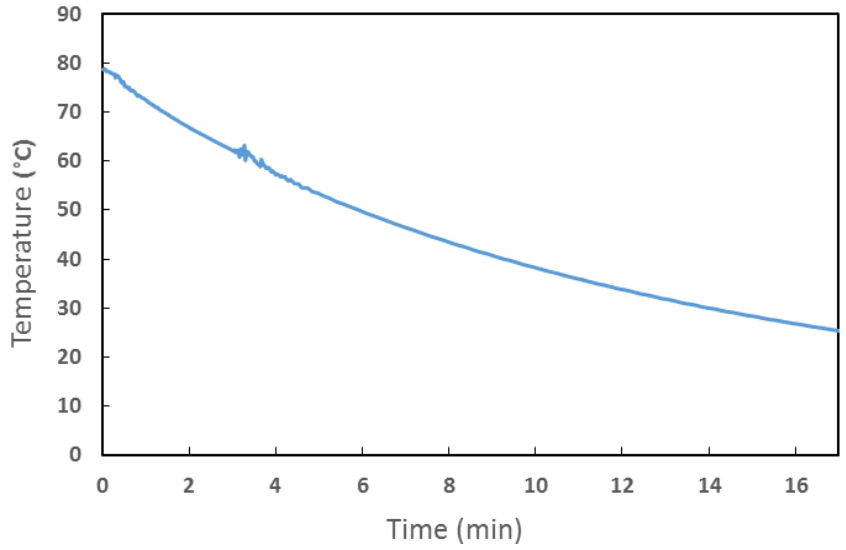

Figure 10 - Average cooling rate for 3 RC samples from 80 ℃ to room temperature (25 ℃) for pH 7.5 test.

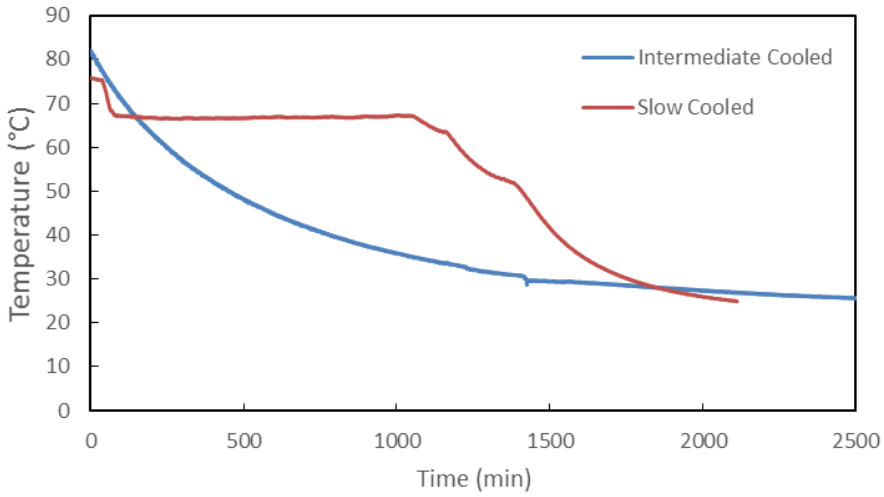

Figure 11 - IC sample and averaged cooling rate for 3 SC samples from 80 ℃ to room temperature (25 ℃) for pH 7.5 test. Oven was turned from 65°C to off at 1300 min.

3103/3203- Cooling Profile

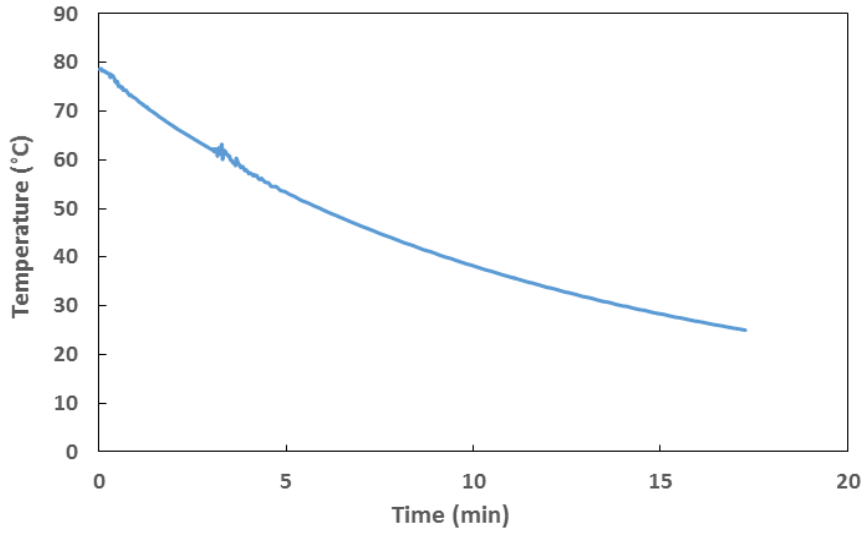

Figure 12 - Average cooling rate for 3 RC samples from 80 ℃ to room temperature (25 ℃) for pH 7.5 test.

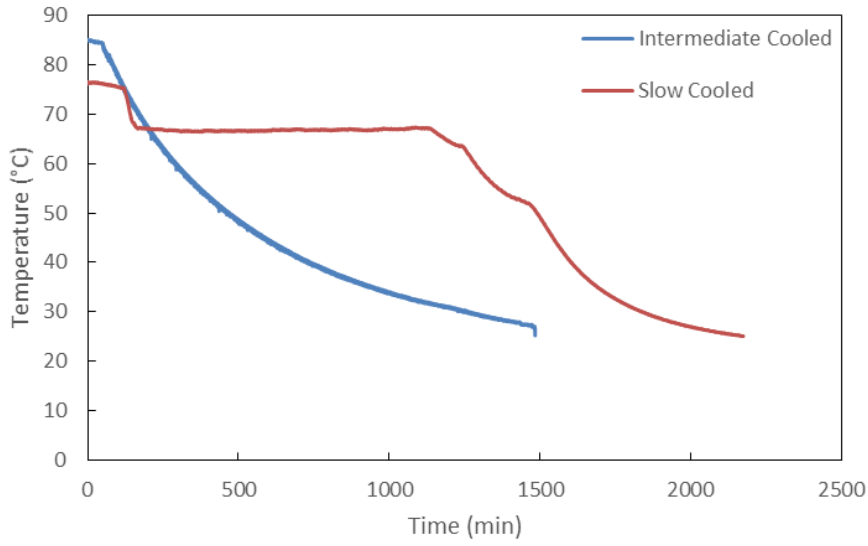

Figure 13 - IC rate and average cooling rate for 3 SC samples from 80 ℃ to room temperature (25 ℃) for pH 7.5 test. Oven was turned from 65°C to off at 1300 min.

3103R/3203R- Cooling Profile

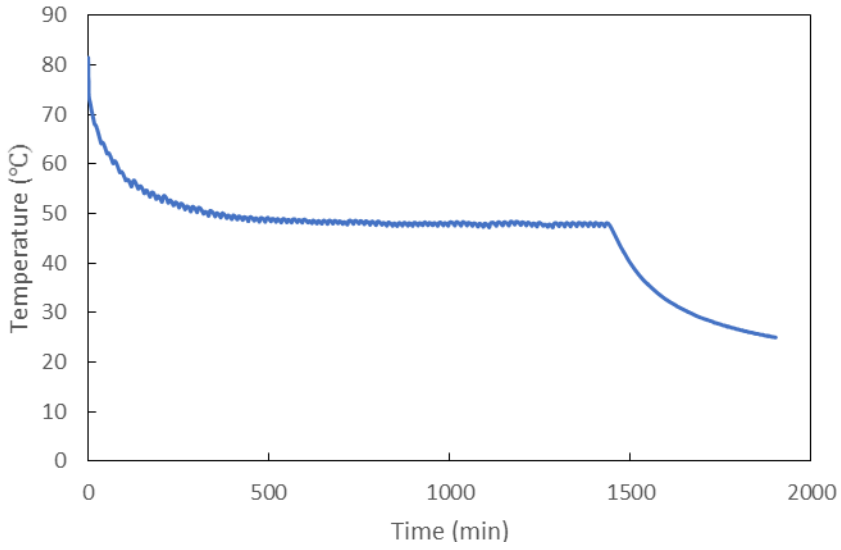

Figure 14 - Average cooling rate for 2 SC samples from 80 ℃ to room temperature (25 ℃) for pH 8.2 repeat test. Oven was turned from 50°C to off at 1400 min.

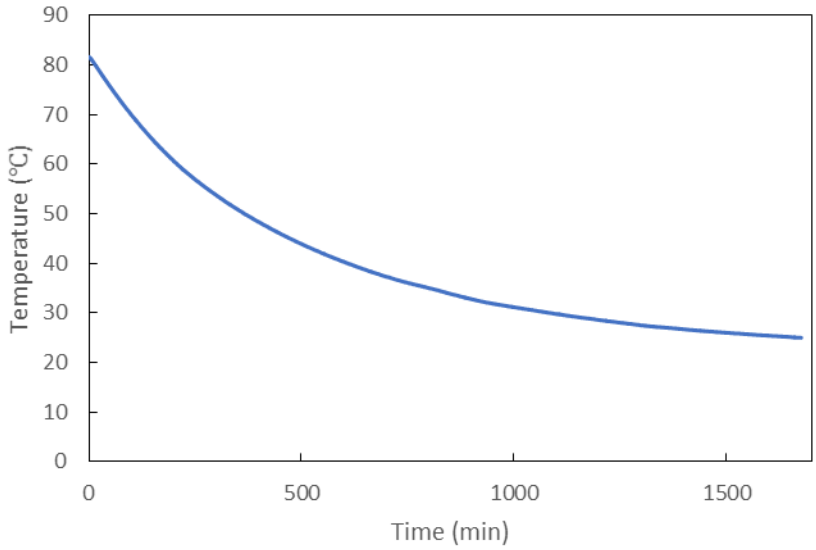

Figure 15 - IC rate from 80 ℃ to room temperature (25 ℃) for pH 8.2 repeat test.

Dissolved Aluminum Concentration via ICP-MS

The samples run through the Perkin Elmer NexIon 300D ICP Mass Spectrometer were taken directly from the corrosion tank before cooling rate samples were taken to verify the final concentration of dissolved aluminum in all sample solutions. The concentrations were 48.12mg/L, (σ = 0.35 mg/L), 69.02 mg/L (σ = 0.38 mg/L), 75.29mg/L (σ = 0.39 mg/L), and 35.6 mg/L (σ = 3.5 mg/L) for the pH 7.2, 7.5, 8.2 and 8.2 repeat tests respectively. For the first test (3101/3201 series), two samples were run through the ICP-MS to ensure homogeneity throughout the aqueous sample. The ICP-MS results of the two samples are compiled in Table 7 for this particular test. Due to the low relative standard deviation (RSD) between the two samples analyzed for the 3101/3102 test series, subsequent test samples were only run once due to cost restrictions.

3101/3201 Test Series ICP-MS Aluminum Concentration Summary

Table 7 - ICP-MS results for 3101/3201 test series.

Sample Name:	**Concentration**	**Standard Deviation**	**% RSD**
Sample 1	47.77 mg/l	1.97 mg/l	4.09%
Sample 2	48.46 mg/l	1.91 mg/l	3.97%
Average	48.12 mg/l	1.94 mg/l	-

Turbidity Measurements

Figure 16 - Figure 19 below shows the results for turbidity vs. cooling rates for all 3000 series tests. It should be noted that turbidity was measured periodically over the course of the following month after each test to ensure that the particle size was stable and did not demonstrate any substantial deviation from the first measurement.

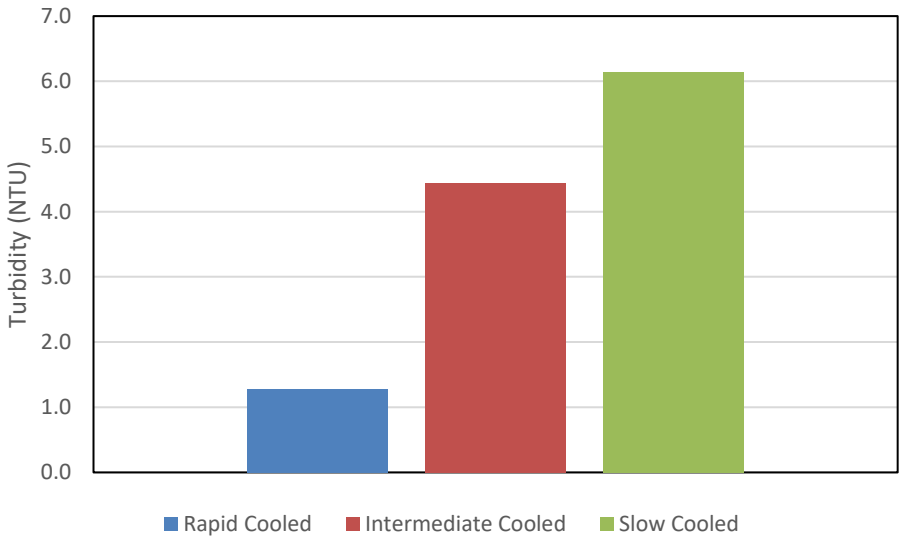

Figure 16 - pH 7.2 sample turbidity based on cooling rate.

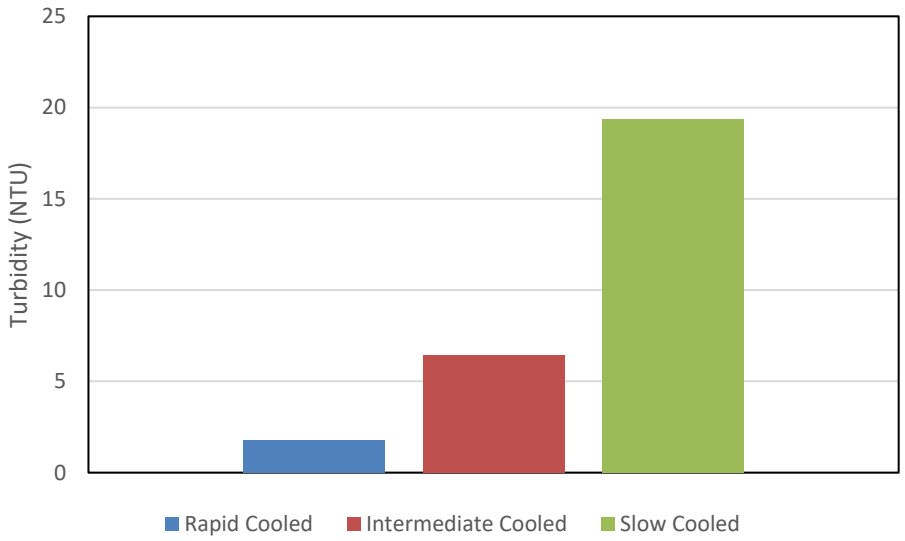

Figure 17 - pH 7.5 sample turbidity based on cooling rate.

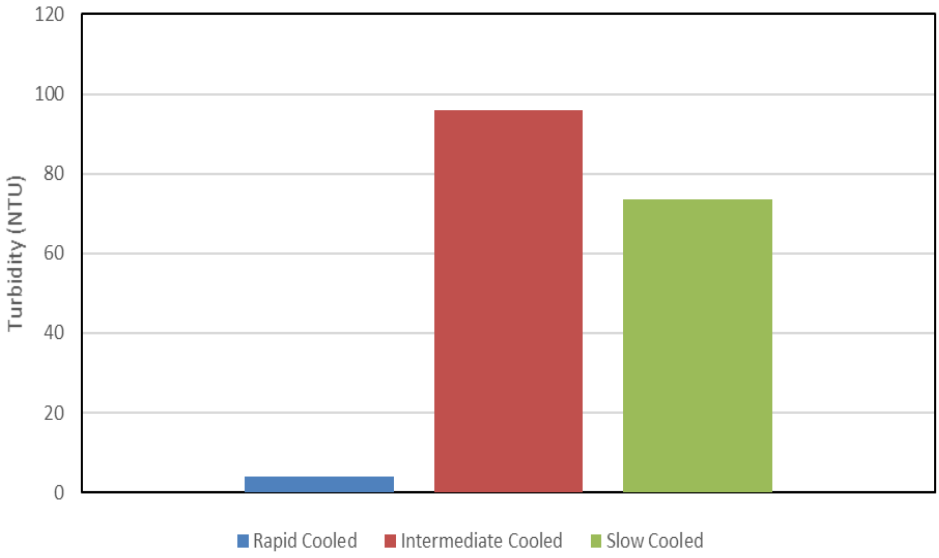

Figure 18 - pH 8.2 sample turbidity based on cooling rate.

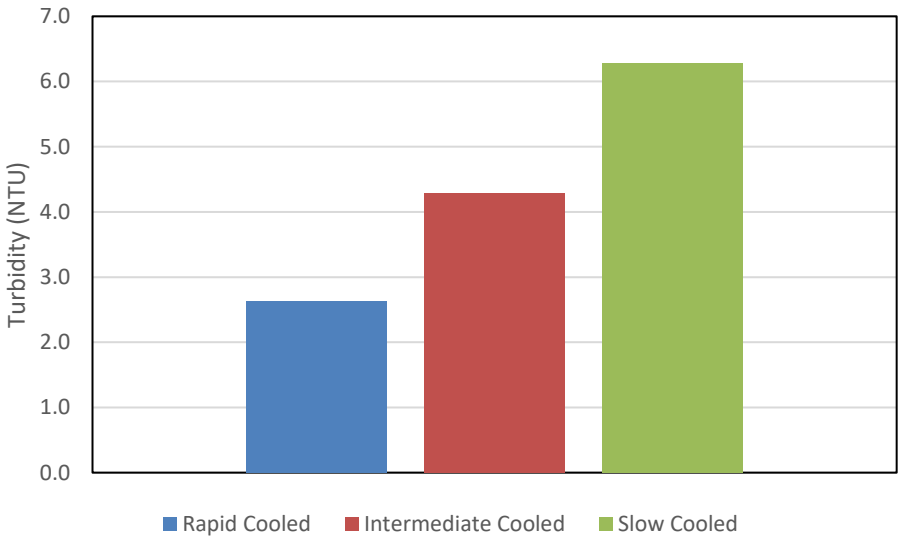

Figure 19 - pH 8.2 repeat sample turbidity based on cooling rate.

The 3101/3201 and 3102/3202 tests started with a solution that was clear after initial chemical dissolution. After corrosion and post cool down, the tank solution had a minimal and almost unobservable change in opacity. This was not however the case with the 3103/3203 test. After cooldown, the solution had a very turbid white appearance as seen in Figure 20. Some of this solution was saved and later decanted in an attempt to acquire a solid concentrated sample for additional analysis.

Figure 20 - 3103/3203 IC solution after initial Al coupon addition (top) and post cooldown (bottom)

Particle Size Characterization and Comparison

The particle size summary is listed in Table 8 for the 3000 series tests. For each test, the particle size increased with a decreasing cooling rate.

Table 8 - Sample precipitate size averaged over three sample runs.

Sample Name	Size 1 (nm)	Volume Percent of Size 1	Standard Deviation (nm)	Size 2 (nm)	Volume Percent of Size 2	Standard Deviation (nm)
RC (7.2)	13.2	99.40%	2.5	-	-	-
IC (7.2)	32.6	85.20%	16.6	5180.0	12.40%	764.5
SC (7.2)	42.7	82.70%	21.7	5244.0	14.90%	732.3
RC (7.5)	11.7	99.80%	4.0	-	-	-
IC (7.5)	33.4	88.90%	19.0	4254.0	8.50%	1235.0
SC (7.5)	74.4	90.70%	46.9	-	-	-
RC (8.2)	19.1	98.87%	5.8	170.0	1.13%	52.36
IC (8.2)	48.1	50.10%	12.2	407.1	49.90%	174.6
SC (8.2)	148.5	56.70%	72.1	227.9	43.30%	95.02

3101/3201 - Particle Size Results

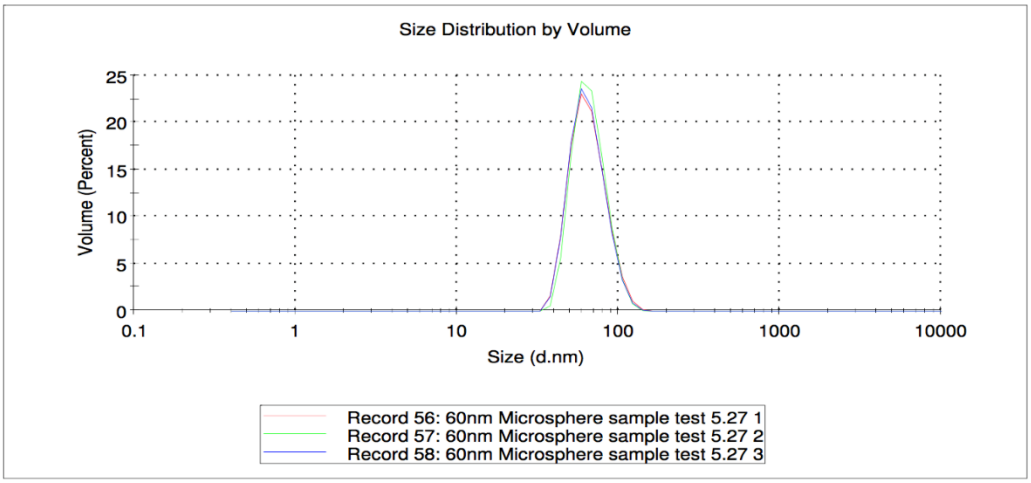

Figure 21 - Particle size distribution for three independent runs of the 60nm microsphere standards for 3101/3201 test series (d.nm = particle diameter in nm).

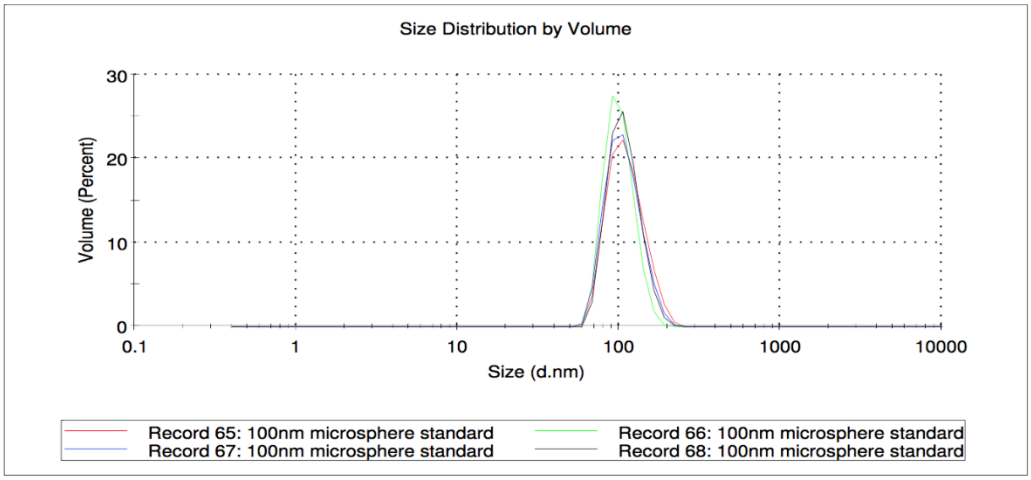

Figure 22 - Size distribution for 4 independent runs of the 100nm standard for the 3101/3201 test series (d.nm = particle diameter in nm).

The graphs in Figure 21 and Figure 22 represent the size distribution for 3 and 4 independent runs of the 60 nm polystyrene microsphere standard and the 100nm standards respectively. The distribution of the particles falls within Malvern's range for the instrument's limitations as well as for the expected variation in the polystyrene standards according to the manufacturer. The low PDI confirms that the size distribution of particles in the standard is narrow. Malvern recommends using DLS for samples with a PDI between 0 and 0.7 for most accurate results with the lower numbers being more accurate. Table 9 shows the size standards run through the instrument prior to testing. Figure 23 to Figure 25 show the full size distribution for the 3101/3201 series test for each sample run.

Table 9 - Size summary for standards run for 3101/3201 test series.

Sample	**Size (nm)**	**Standard Dev (nm)**	**PDI**
60nm Standard	65.67	16.36	0.007
100nm Standard	108.7	24.73	0.076

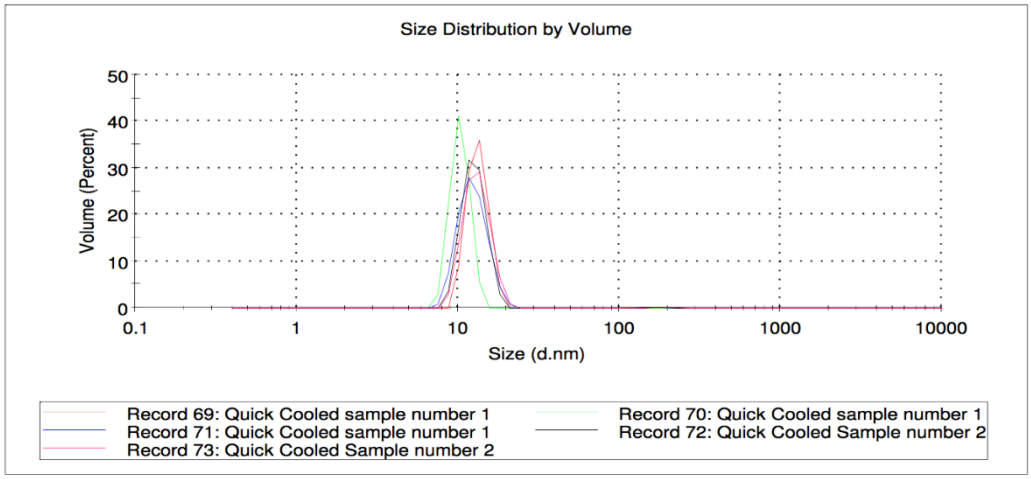

Figure 23 - Particle size distribution for two separate RC samples for pH 7.2 test (d.nm = diameter in nm).

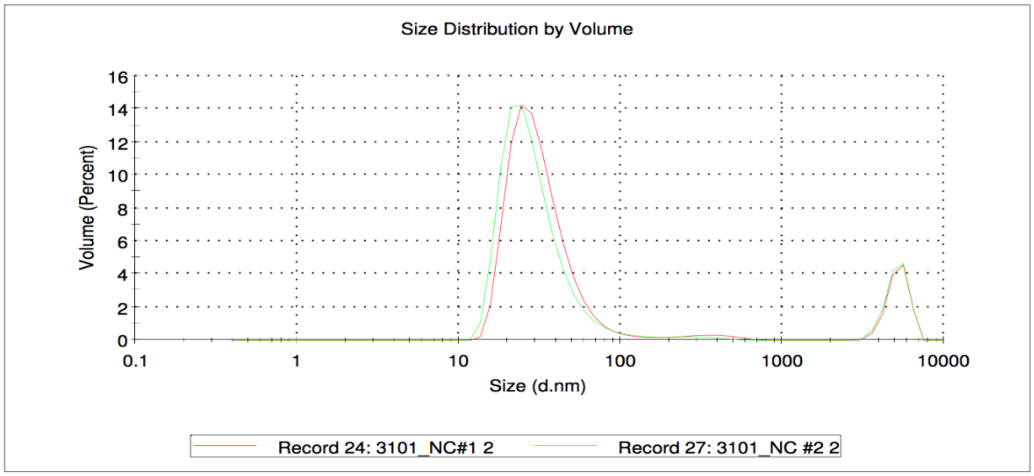

Figure 24 - Particle size distribution for two independent runs of the IC sample for pH 7.2 test (d.nm = diameter in nm).

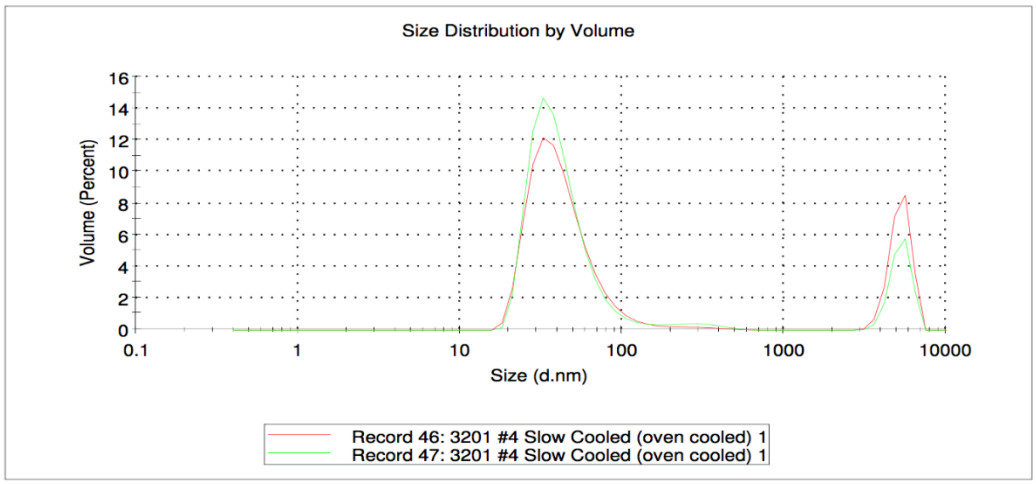

Figure 25 - Particle size distribution for the SC samples for pH 7.2 test (d.nm = diameter in nm).

Table 9 shows that there is an apparent shift in the mean diameter correlated to the decreased cooling rate. This conforms to the turbidity results in the previous section. Figure 24 and Figure 25 also show that the slower cooling rates tend to form two distinct particle sizes as opposed to a discreet precipitate size as seen for the RC samples.

3102/3202 - Particle Size Results

The results from the NIST standards on the Zen 3000 for the 3102/3202 test are presented in Figures 26 and Figure 27 and summarized in Table 10.

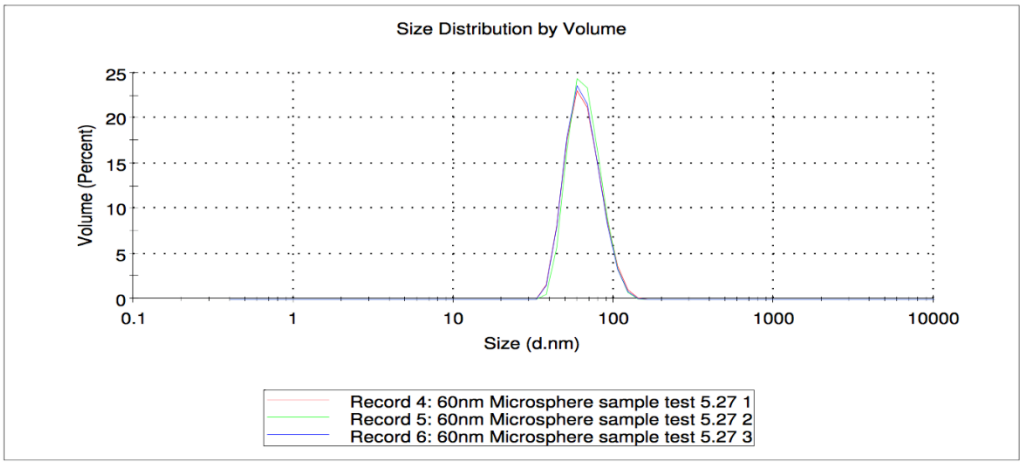

Figure 26 - Size distribution for three independent runs of the 60nm microsphere standards for the 3102/3202 test series (d.nm = particle diameter in nm).

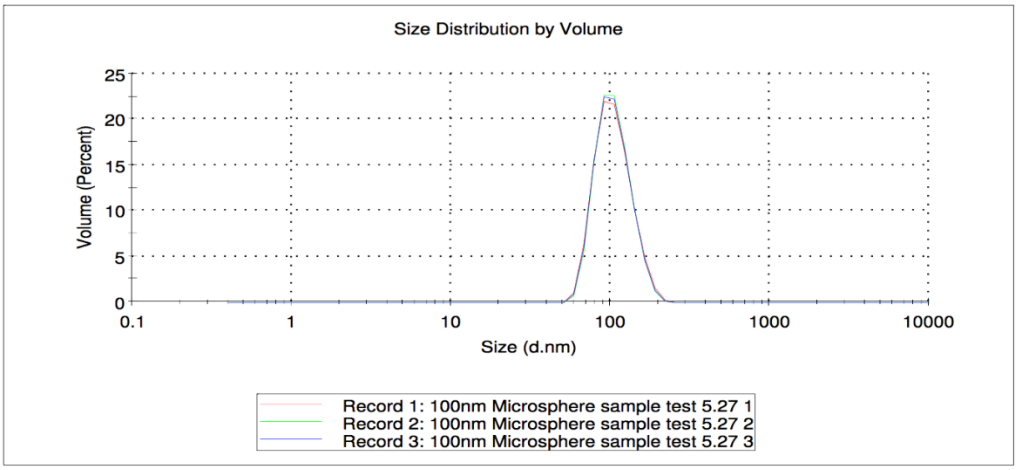

Figure 27 - Size distribution for 3 independent runs of the 100nm standard for the 3102/3202 test series (d.nm = particle diameter in nm).

Figure 27 illustrates the size distribution for three independent runs of the 60 nm polystyrene microsphere standard and the 100nm standards for the 3201/3202 test series. The distribution of the particles falls within Malvern's range for the instrument's limitations as well as for the expected variation in the polystyrene standards according to the manufacturers. The low PDI seen below confirms that the size distribution of particles in the sample is narrow. Figure 28 -Figure 32 shows the full size profiles for the samples run during the 3102/3202 test.

Table 10 - 3102/3202 size summary for standards.

Sample	Size (nm)	Standard Dev (nm)	PDI
60nm Standard	66.11	16.92	0.019
100nm Standard	106.4	27.58	0.022

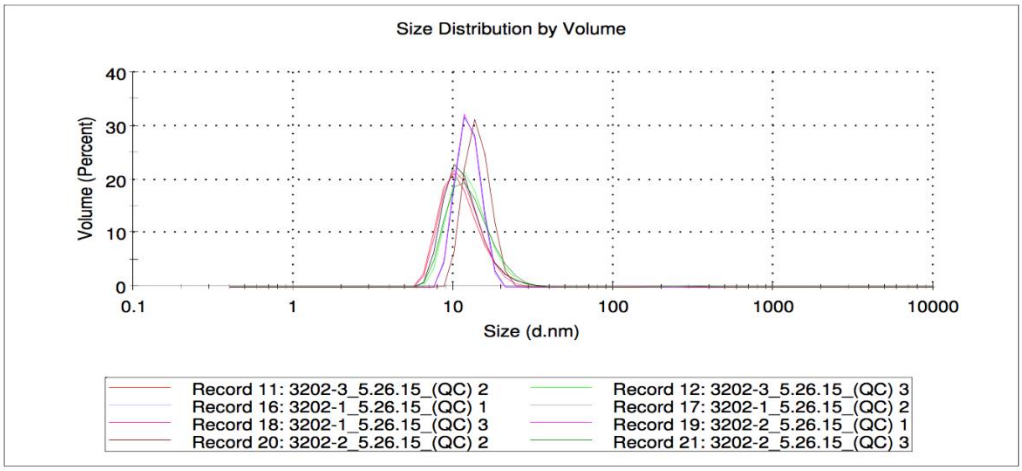

Figure 28 - Particle size distribution for three separate RC samples (d.nm = diameter in nm).

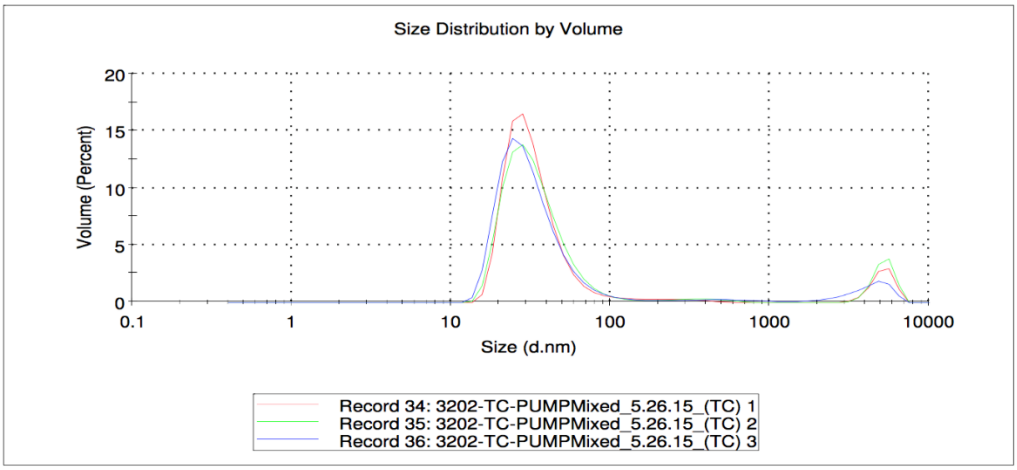

Figure 29 - Particle size distribution for IC sample (d.nm = diameter in nm).

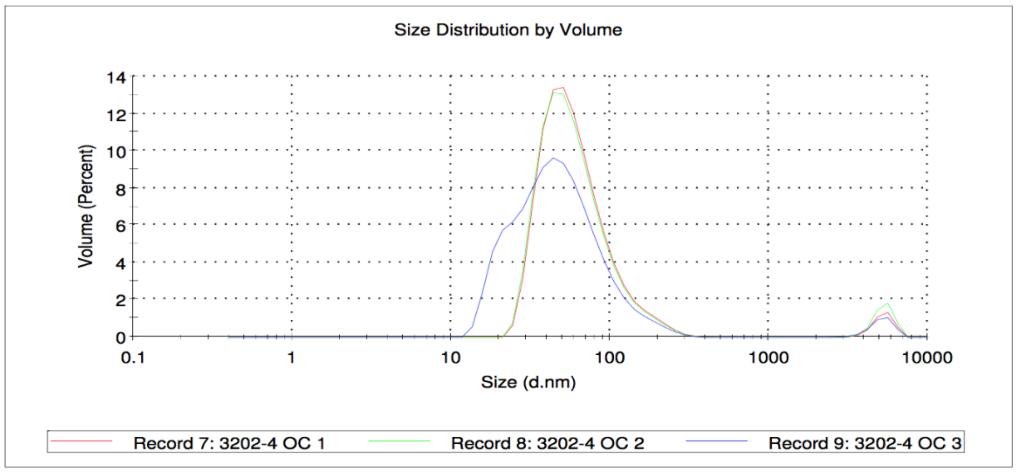

Figure 30 - Particle size distribution for SC sample 1 (d.nm = diameter in nm).

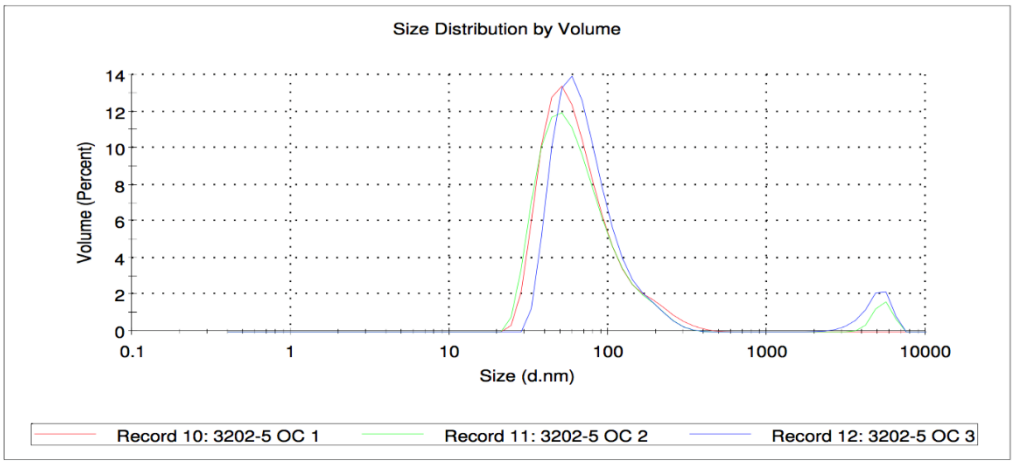

Figure 31 - Particle size distribution for SC sample 2 (d.nm = diameter in nm).

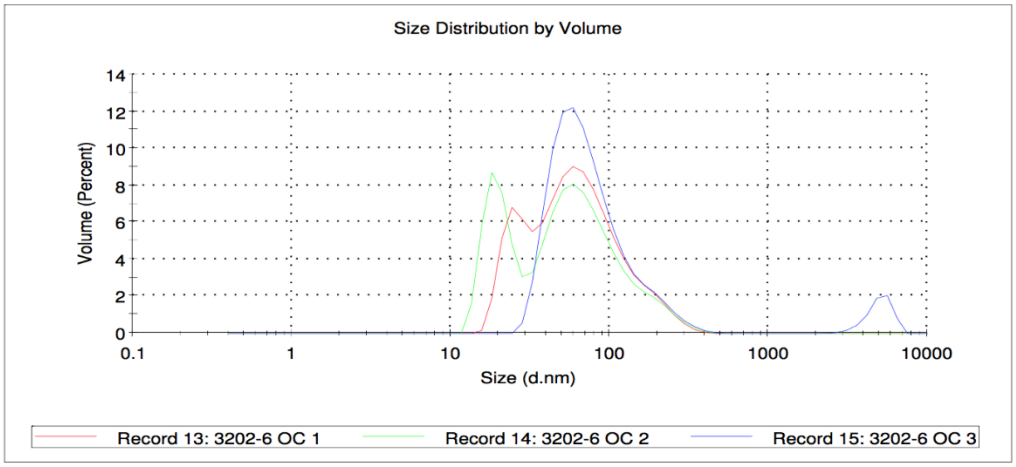

Figure 32 - Particle size distribution for SC sample 3 (d.nm = diameter in nm).

3103/3203 Particle Size Results

The results from the NIST standards on the Zen 3000 for the 3103/3203 test are presented in Figure 33 and Figure 34 below and summarized in Table 11 below.

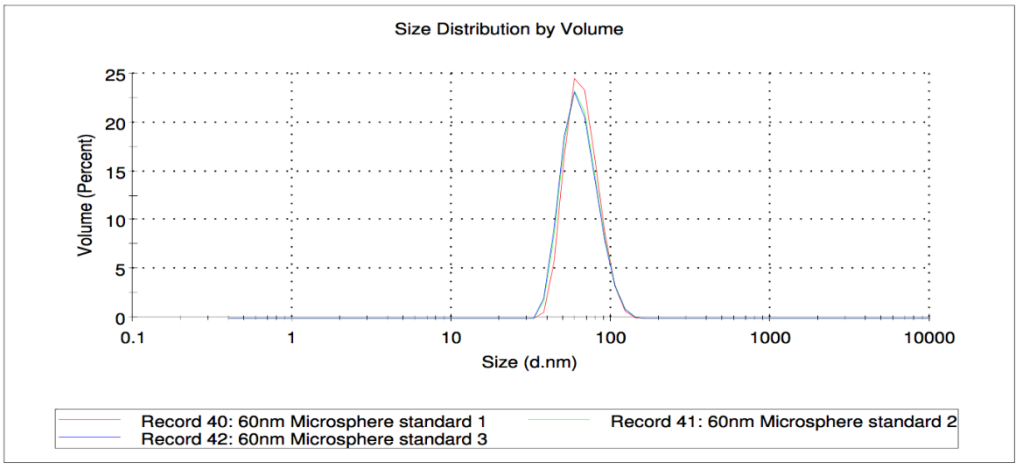

Figure 33 - Size distribution for three independent runs of the 60nm microsphere standards for 3103/3203 test series (d.nm = particle diameter in nm).

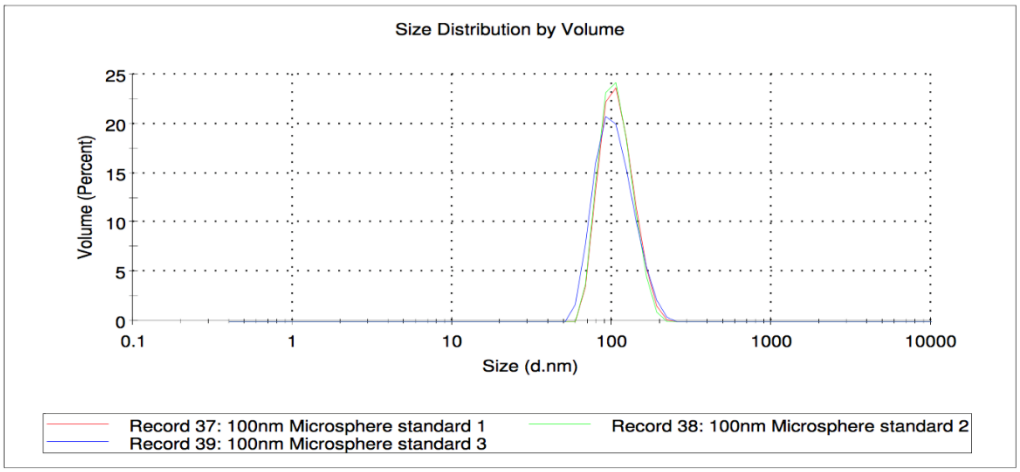

Figure 34 - Size distribution for 3 independent runs of the 100nm standard for 3103/3203 test series (d.nm = particle diameter in nm).

Figure 34 illustrates the size distribution for three independent runs of the 60nm and 100 nm polystyrene microsphere standards. The distribution of the particles falls within Malvern's range for the instrument's limitations as well as for the expected variation in the polystyrene standards according to the manufacturers. The low PDI seen below confirms that the size distribution of particles in the sample is narrow. Figure 35-Figure 41 illustrate the full size profiles for the 3103/3203 test.

Table 11 - 3103/3203 size summary for standards

Sample	Size (nm)	Standard Dev (nm)	PDI
60 nm Standard	64.98	16.71	0.018
100 nm Standard	109.6	26.47	0.019

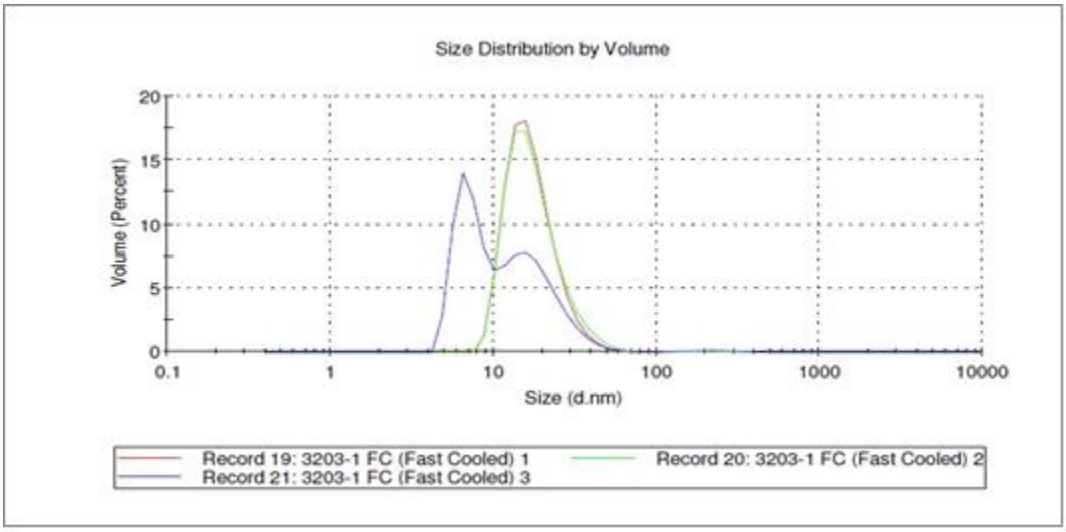

Figure 35 - Particle size distribution for RC sample 1 (d.nm = diameter in nm).

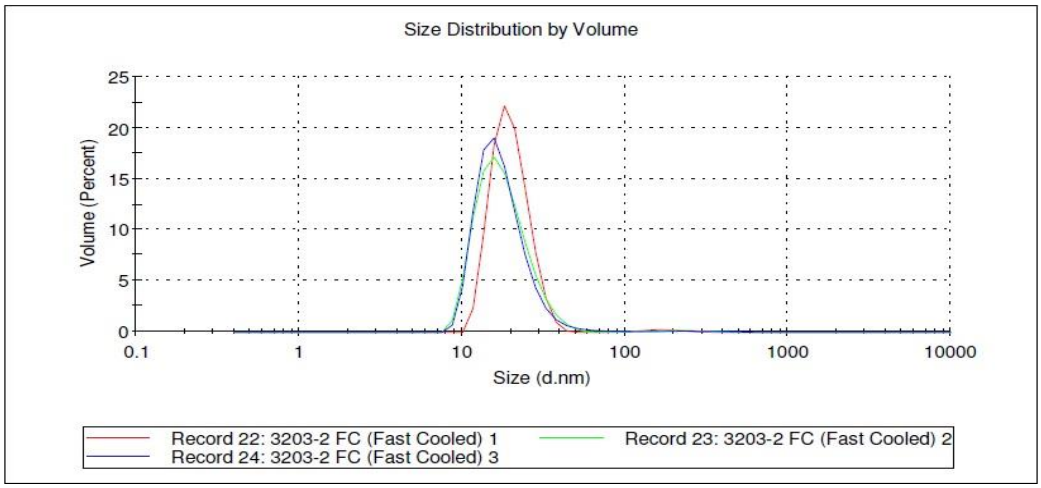

Figure 36 - Particle size distribution for RC sample 2 (d.nm = diameter in nm).

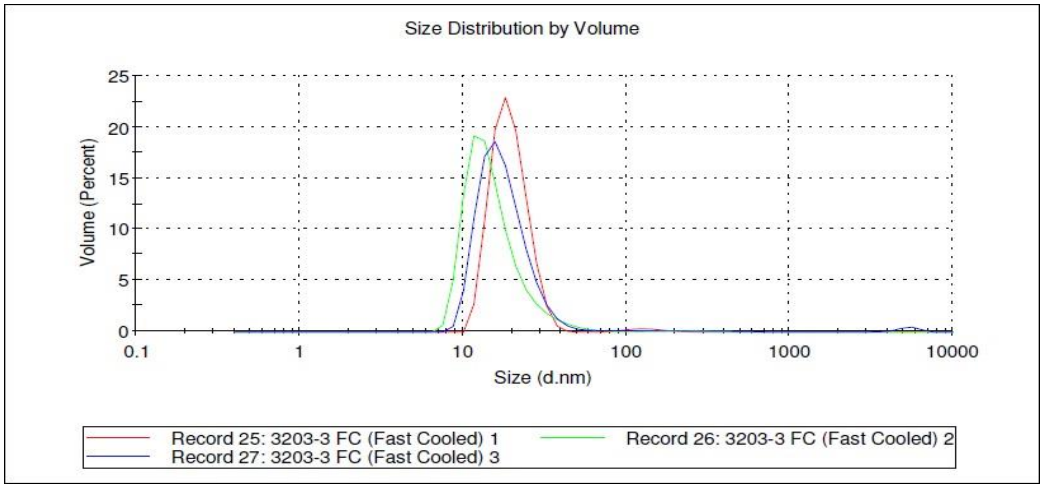

Figure 37 - Particle size distribution for RC sample 3 (d.nm = diameter in nm).

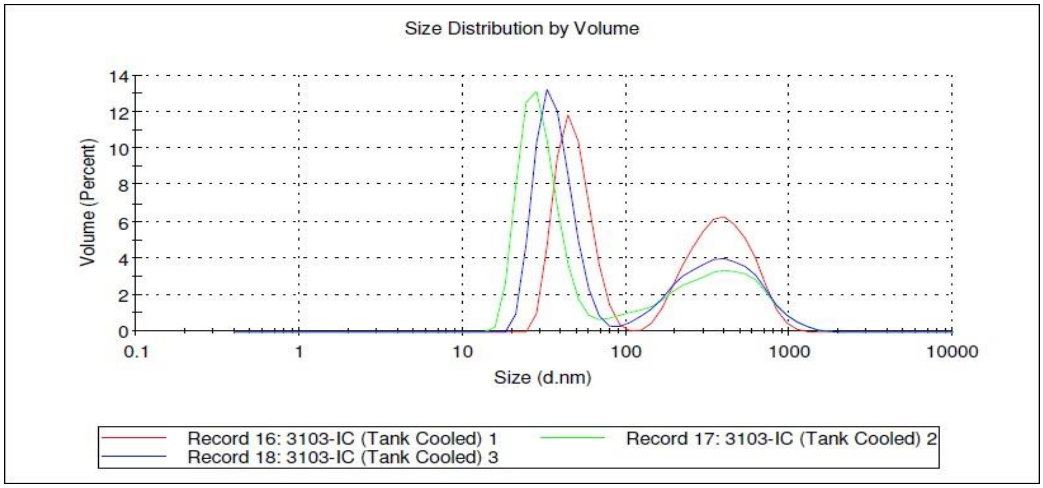

Figure 38 - Particle size distribution for IC sample (d.nm = diameter in nm).

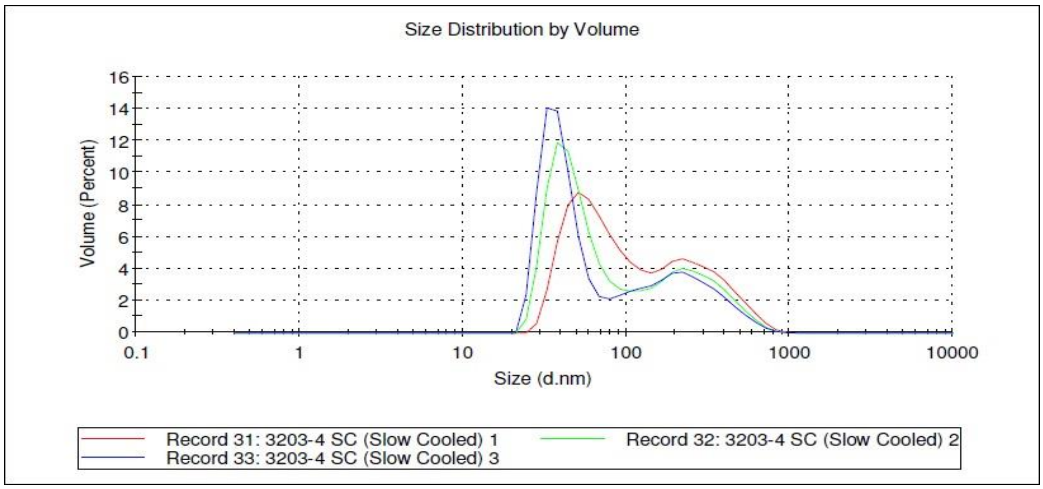

Figure 39 - Particle size distribution for SC sample 1 (d.nm = diameter in nm).

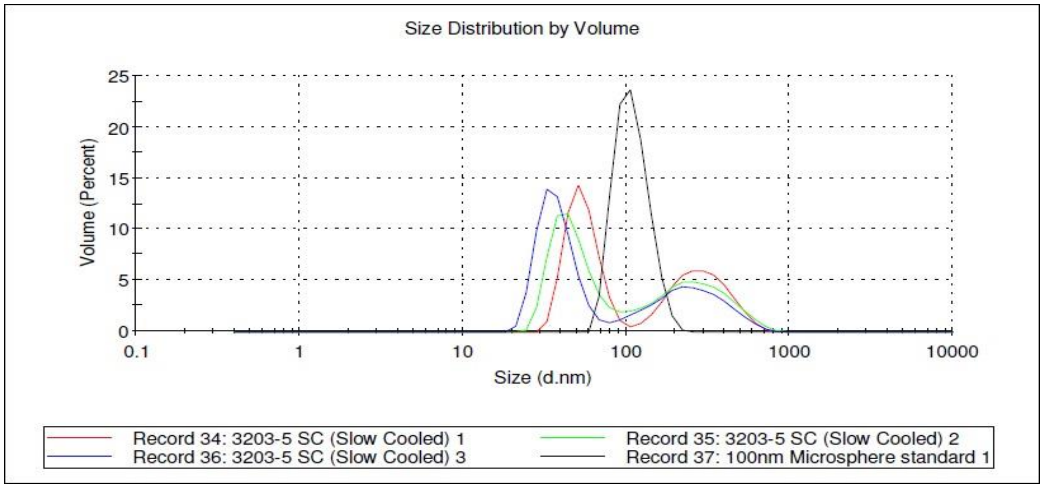

Figure 40 - Particle size distribution for SC sample 2 (d.nm = diameter in nm).

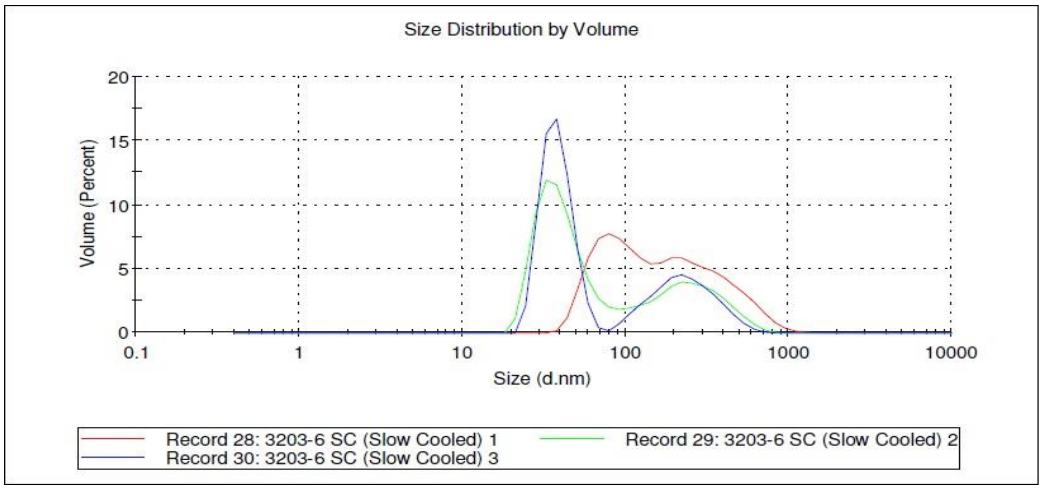

Figure 41 - Particle size distribution for SC sample 3 (d.nm = diameter in nm).

1100 Particle Size Results

The WCAP precipitate was measured for size and 87% of the particles were determined to have a mean diameter of 3785 nm (±1533nm) and the remaining 13% with a mean diameter of 481 nm (±179 nm). The settling characteristics over the first hour were inconclusive and no visible settling occurred. This result was consistent with settling tests performed with the corrosion product precipitate settling tests as well.

The results from the NIST standards on the Zen 3000 for the 1100 test are presented in Figure 42 and Figure 43 and are summarized in Table 12 below.

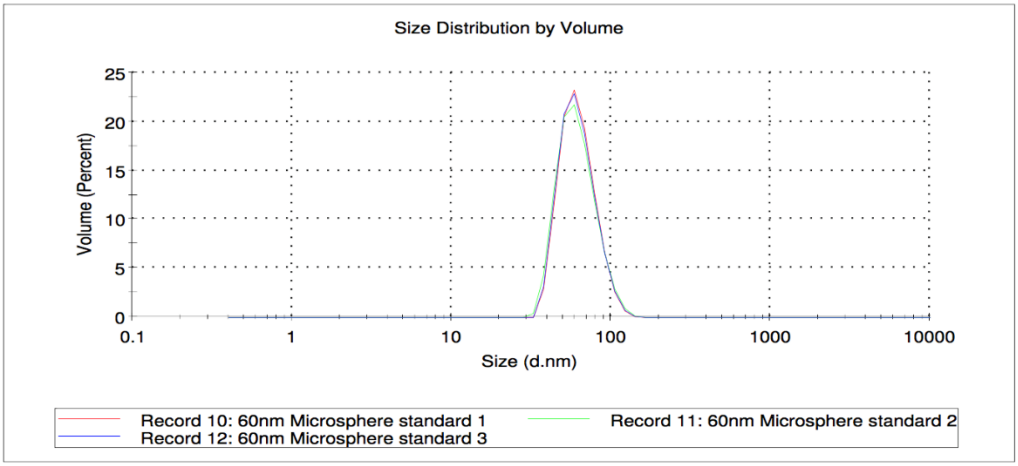

Figure 42 - Size distribution for three independent runs of the 60nm microsphere standards (d.nm = particle diameter in nm).

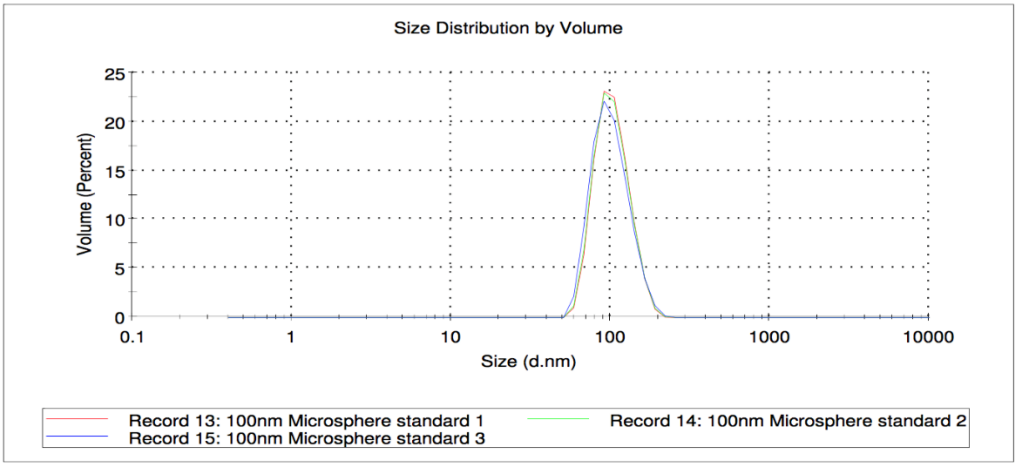

Figure 43 - Size distribution for 3 independent runs of the 100nm standard (d.nm = particle diameter in nm).

Figure 43 illustrates the size distribution for three independent runs of the 60 nm and 100nm polystyrene microsphere standards for the 1100 test series. The distribution of the particles falls within Malvern's range for the instrument's limitations as well as for the expected variation in the polystyrene standards according to the manufacturers. The low PDI seen below confirms that the size distribution of particles in the sample is narrow.

Table 12 - Size summary for standards for 1100 test.

Sample	Size (nm)	Standard Dev (nm)	PDI
60nm Standard	63.0	16.12	0.022
100nm Standard	104.4	25.35	0.020

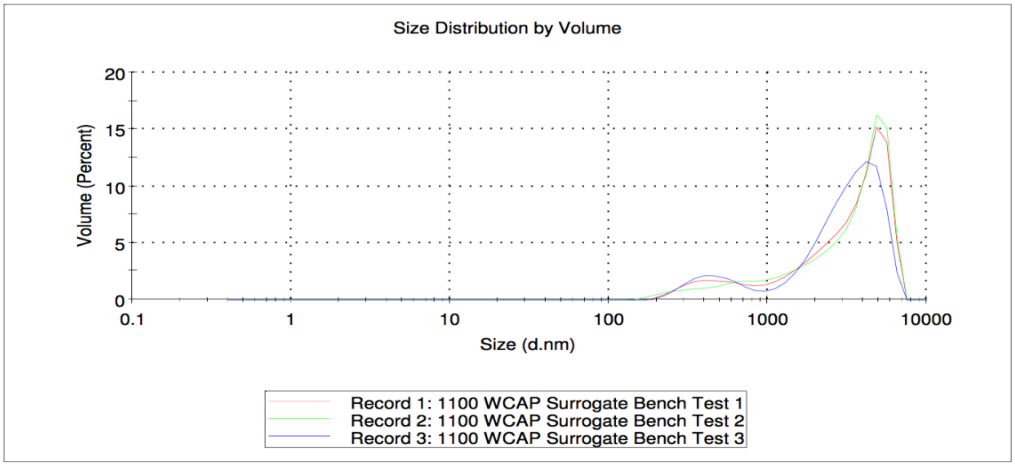

Figure 44 - Particle size distribution for the WCAP surrogate aluminum precipitate (d.nm = diameter in nm).

Table 13 - 1100 test WCAP average particle size distribution summary.

Sample Name	Size 1 (nm)	Volume percent of size 1	Standard Deviation (nm)	Size 2 (nm)	Volume percent of size 2	Standard Deviation (nm)
WCAP Prep (pH 7.2)	3785	86.5%	1533	481.4	13.5%	178.6

TEM Analysis

3101/3201 TEM Results

Analysis of three cooling rates (RC, IC, and SC) were performed with TEM to study precipitate characteristics of interest such as morphology and composition.

Different areas were subject to observation and analysis from the samples selected. Figure 45, Figure 46, and Figure 47 summarize the main observations for selected areas of the RC, IC, and SC samples respectively for the 3101/3201 test. Samples showed aluminum-compound particles of various size, morphology, composition, and crystallography. Graphitic particles and sodium-containing aluminum compounds were also detected (copper and carbon come mainly from the TEM grid).

The analysis conducted on the RC sample showed an amorphous aluminum compound with the intensity Al/O ratio of ~ 0.5 (Figure 45). It should be noted that the image seen in Figure 45 appears to be multiple precipitate particles of a small particle scale in comparison to the slower cooled samples seen in Figure 46 and Figure 47. In Figure 46, (IC sample, area 2), a large particle on a micrometer scale is seen and indexed as a single crystal by the selected-area diffraction pattern. Its surface is at least partially porous. Though particles observed in RC and IC are different in morphology and crystallography they show similar compositional properties. The large particles (a couple of hundreds nanometer in size) shown in Figure 47, (IC sample, area 3), show crystallinity but have a different composition than the other samples. The particles in the SC sample appear to be colloidal in nature forming a larger conglomerate particle. The EDS intensity ratio is around 2 and the surface of the particles appears very smooth. Along the surface of the large particles, and along the edge of the perforated carbon film, there are some additional smaller particles. These may be similar to the particles seen in the RC sample.

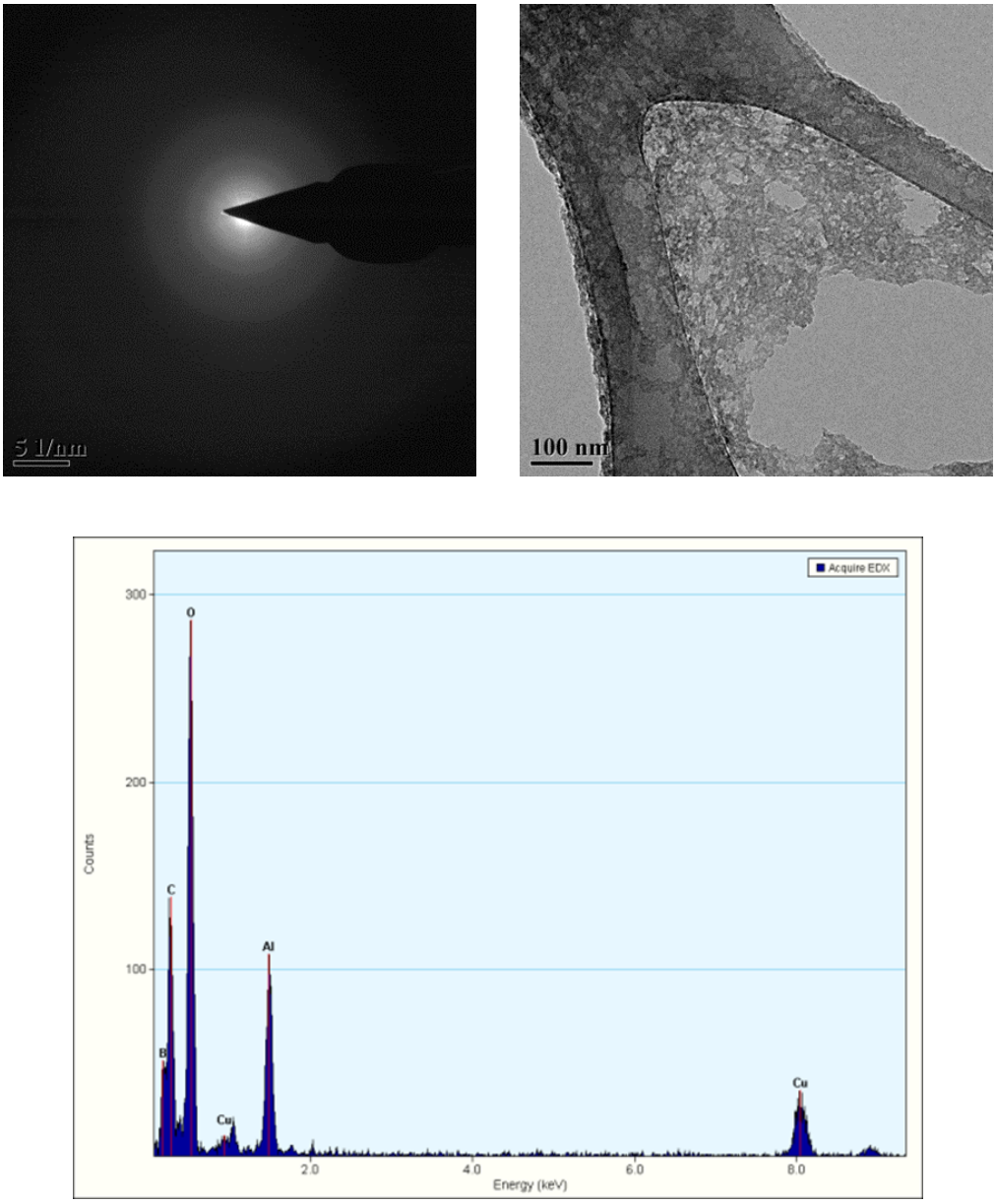

Figure 45 - TEM analysis - rapid cooled (RC) sample (area 2).

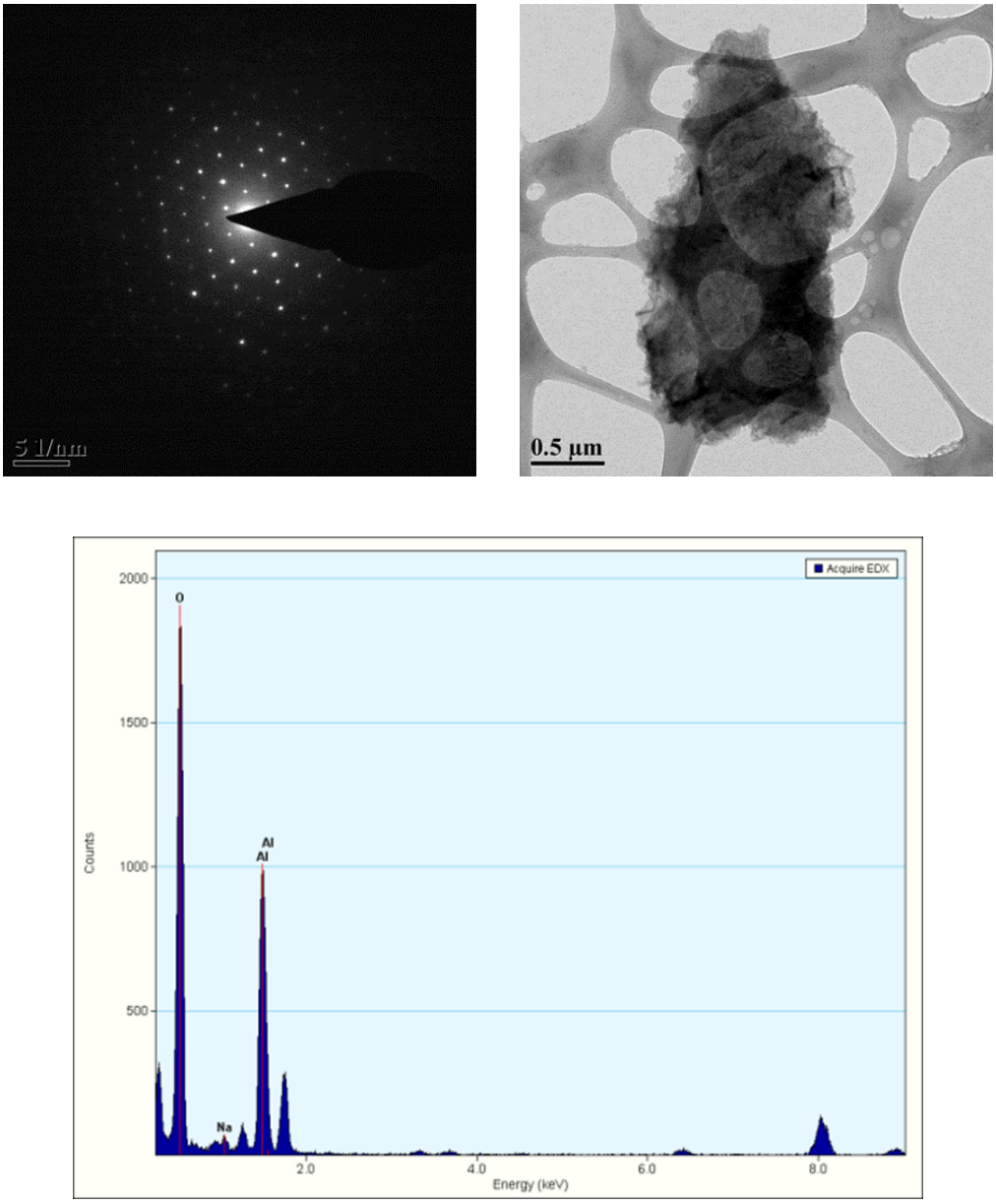

Figure 46 - TEM analysis - IC sample (area 2) for pH 7.2 test.

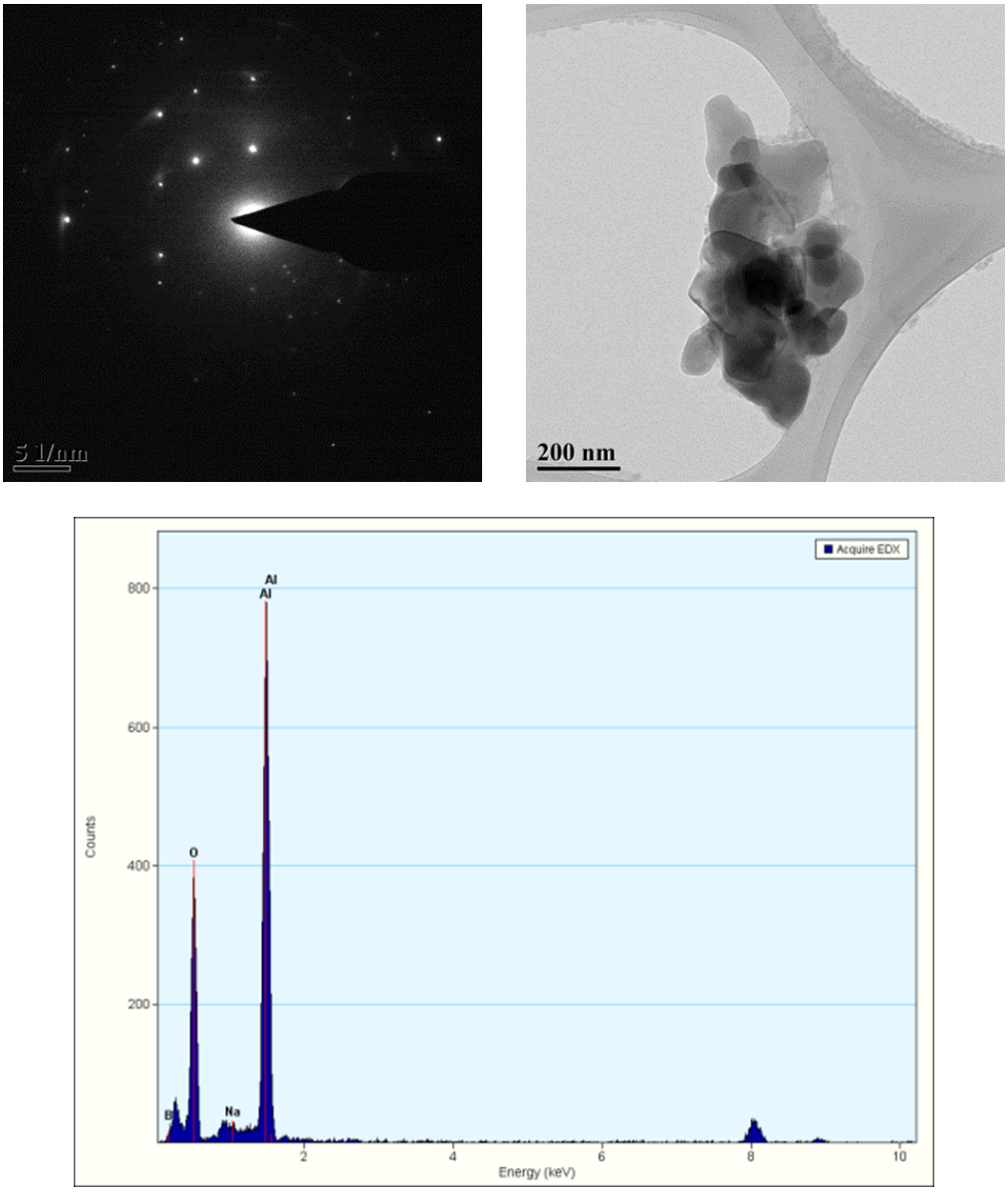

Figure 47 - TEM analysis - IC sample (area 3) for pH 7.2 test.

Table 14 - RC sample composition (area 2) for pH 7.2 test.

Element	Weight %	Atomic %	Uncertainty %
B	41.45	53.22	3.6
O	47.18	40.93	1.13
Al	11.35	5.83	0.40

Table 15 - IC sample composition 2 for pH 7.2 test.

Element	Weight %	Atomic %	Uncertainty %
B	28.63	39.80	1.00
O	53.24	49.99	0.46
Na	1.18	0.77	0.05
Al	16.93	9.43	0.19

Table 16 - IC sample composition (area 3) for pH 7.2 test.

Element	Weight %	Atomic %	Uncertainty %
B	7.16	12.79	1.09
O	42.01	50.73	0.81
Na	0.64	0.54	0.05
Al	50.17	35.92	0.62

EDS cannot detect hydrogen so the exact compositional information cannot be confirmed. However, since the ratio of Al to O is 0.5 for AlOOH and 0.67 for Al_2O_3, it may be plausible to think that the RC sample may have produced a single AlOOH compound and the slower cooling rates may have produced two different Al compounds, (both in amorphous and crystalline structure) namely as Al_2O_3.

It should be noted that due to the low concentration of aluminum in the samples analyzed, statistical analysis was not conducted for this test. In particular, particles shown in Figure 46 and Figure 47 were isolated when performing the scanning and information on the presence of similar particles in the sample analyzed is not reported. The analyses confirmed that the presence of boron did not affect the measurements since concentrations of boron in the areas analyzed were almost undetectable. It has also to be remarked that the intensity peak of the oxygen may be affected by the inevitable presence of this element in atmospheric composition.

3102/3202 TEM Results

The particles for the IC and SC samples for the 3102/3202 test series have a very homogeneous composition. The shapes of the particles observed in the TEM analysis are very similar. This presents the possibility of a similar morphology of the two cooling rates for this particular test. They appear to have an amorphous structure consisting dominantly of aluminum and oxygen. Particles in the RC sample are not homogeneous in morphology, crystallography, or component elements. Thus, they can be either amorphous or crystalline while they often contain sodium or calcium. The specific results from the TEM analysis for this test are detailed in Figure 48, Figure 49 and Figure 50.

The difference between the IC and SC sample is the atomic ratio of O to Al, (~ 6.5 for IC, ~ 4 for SC). The atomic ratios are a lot greater than 1.5 and particles in both samples do not show a typical alumina crystal structure such as an alpha or gamma

phase. Therefore, the particles in the IC and SC samples for this test cannot be Al_2O_3. It is not clear, however, if they are boehmite or diaspore either because the atomic ratios are still much higher than 2. Since the crystalline structure is seen only in the RC sample, the additional elements might play some role in forming the crystalline aluminum structure.

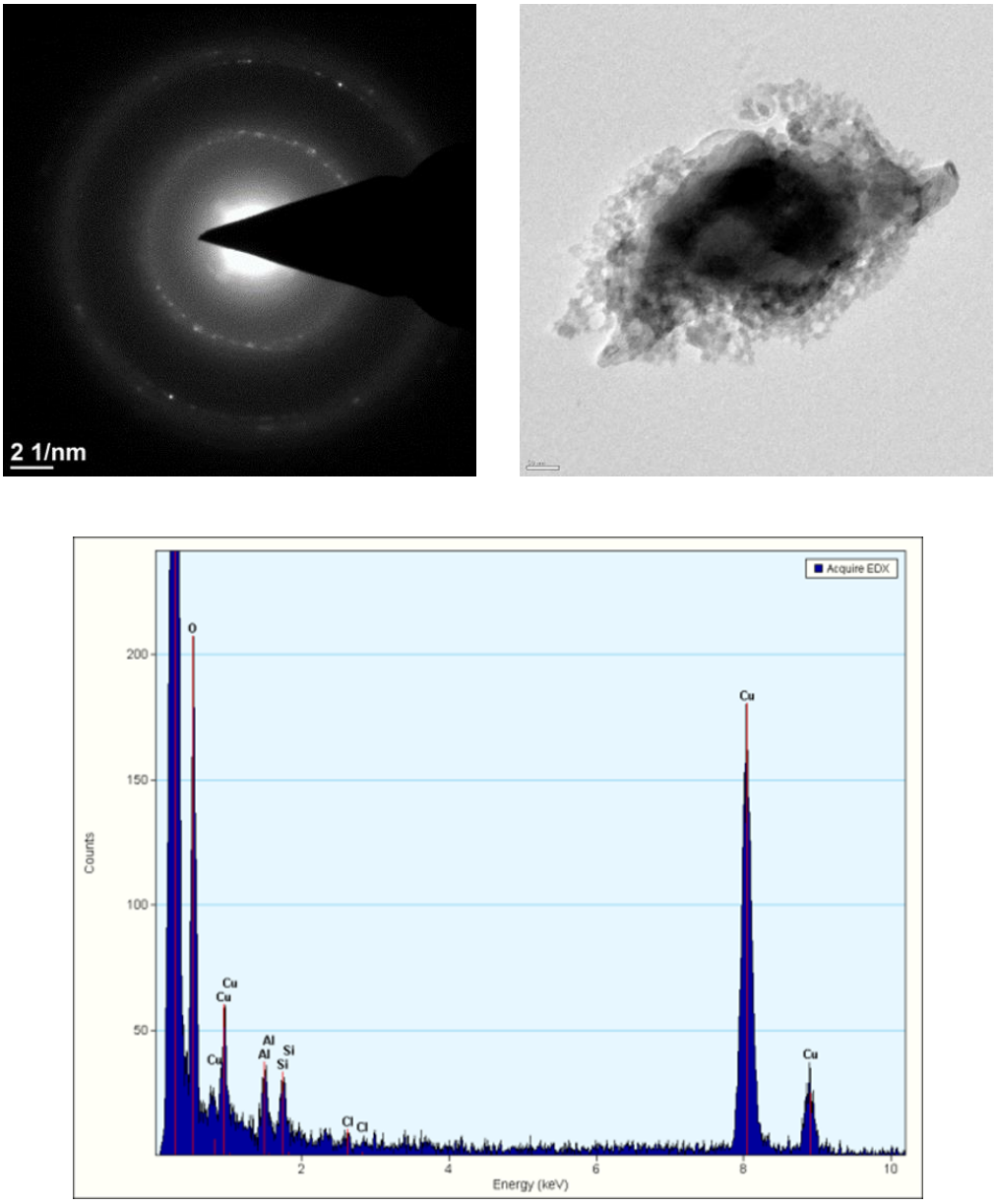

Figure 48 - TEM analysis (RC sample for pH 7.5 test).

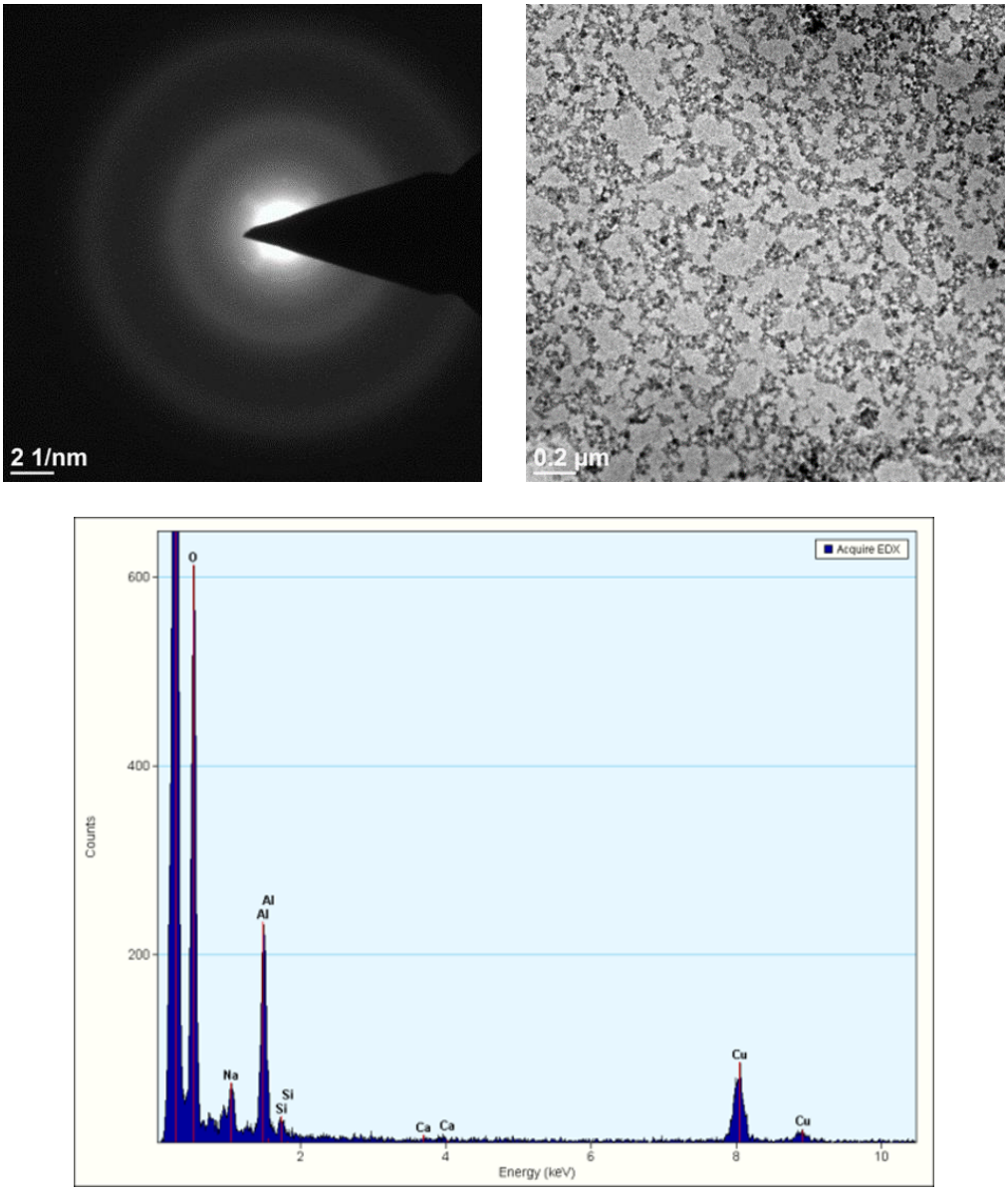

Figure 49 - TEM analysis (IC sample for pH 7.5 test).

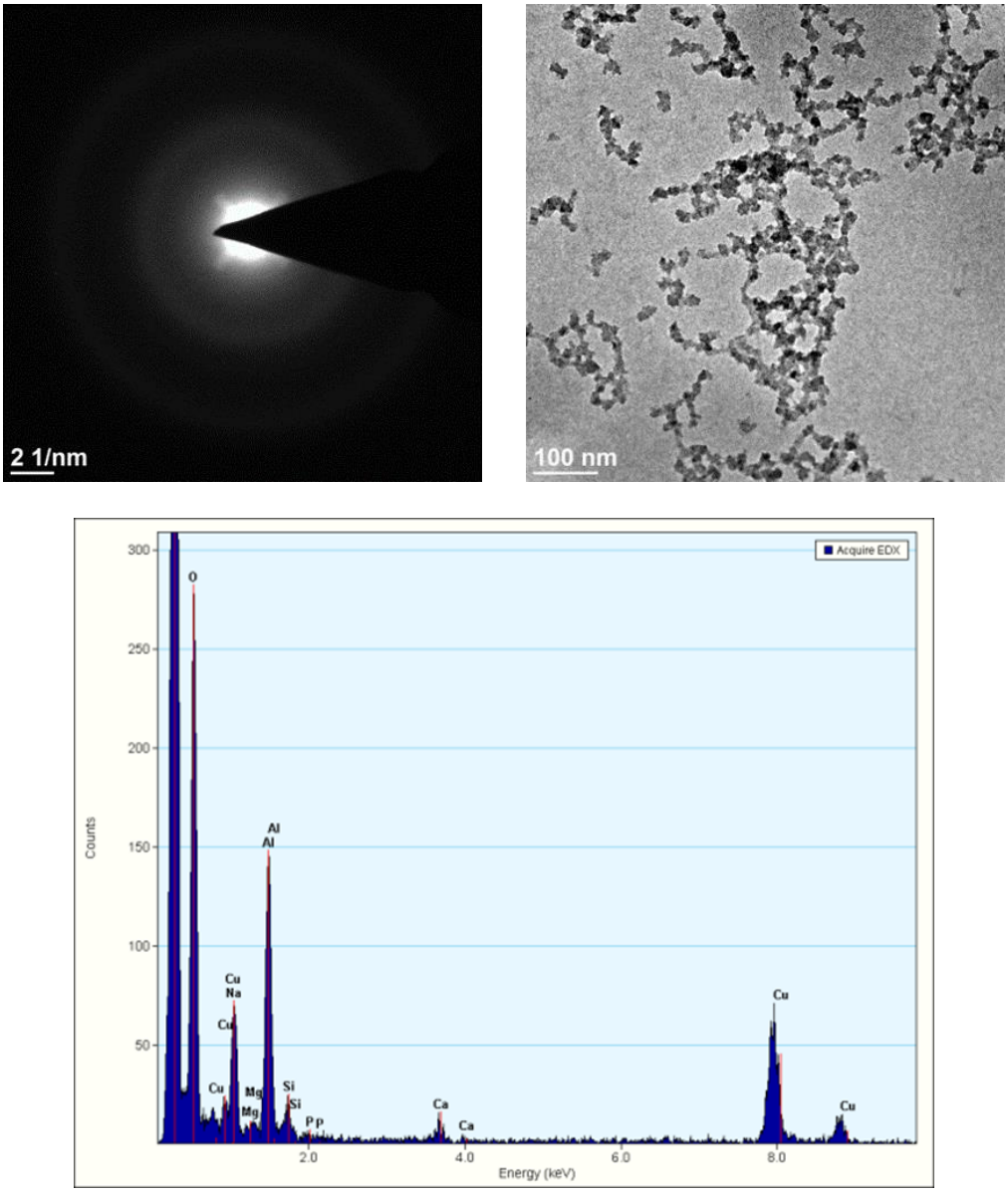

Figure 50 - TEM analysis (SC sample for pH 7.5 test).

3103/3203 TEM Results

The IC sample for the 3103/3203 test series was found to be similar both in morphology and crystallography to the IC and RC samples generated during the 3102/3202 test (pH 7.5). The atomic ratio of O to Al for this sample ranged between 2.7 and 4, which is relatively close to 2 for the Al-O-OH structure.

The RC and SC samples did not show a sharp Al peak however. Measurements of particles in the samples does not suggest a clear indication that they are Al compounds. It is possible to think the unexpected results come from the low concentration of these samples. Since the particles or particle aggregates observed from these samples did not show the Al transition in EDS explicitly, it may be also possible to assume that there is only a very small amount of Al in the samples.

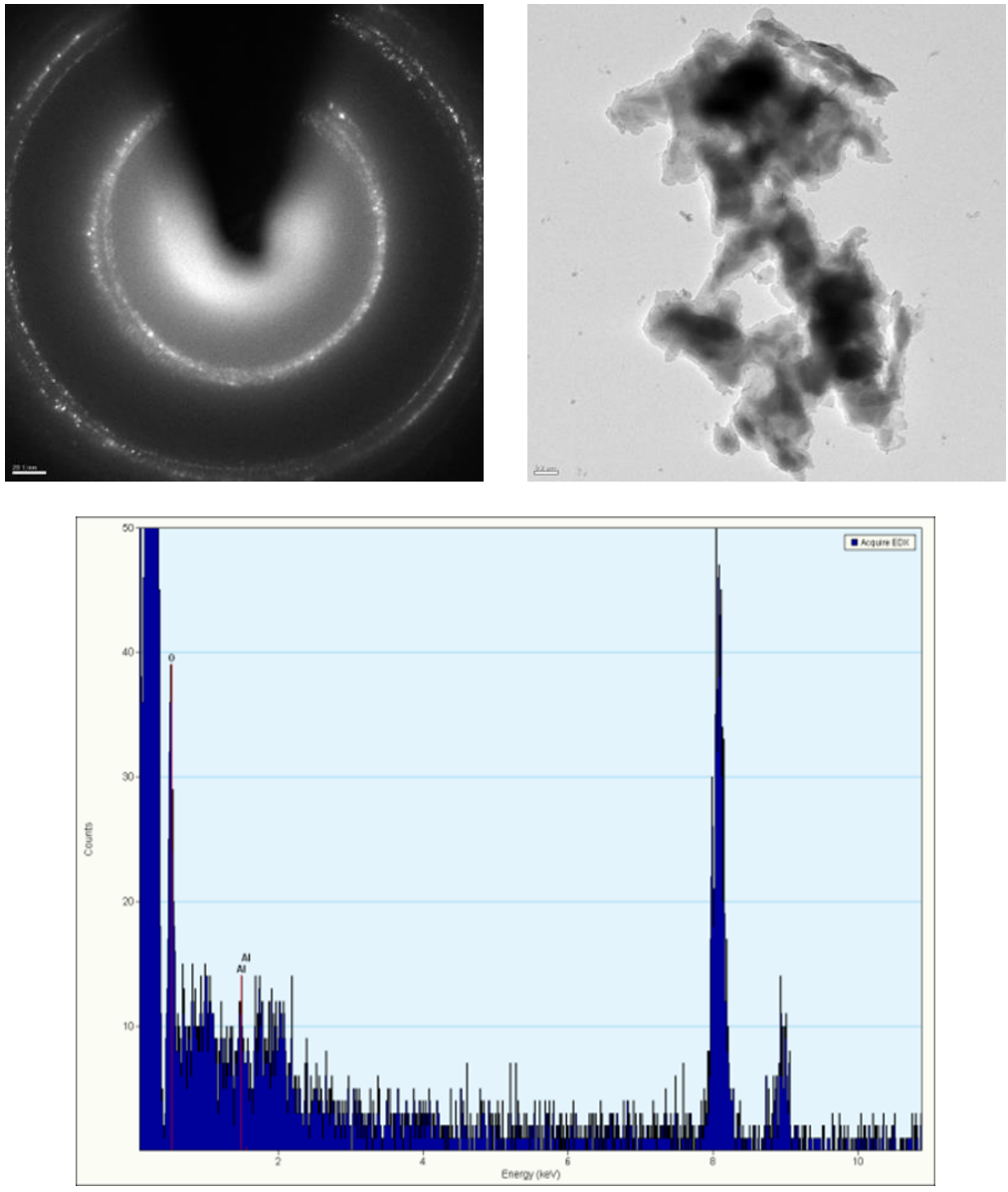

Figure 51 - TEM analysis (RC sample (area 1) for pH 8.2 test).

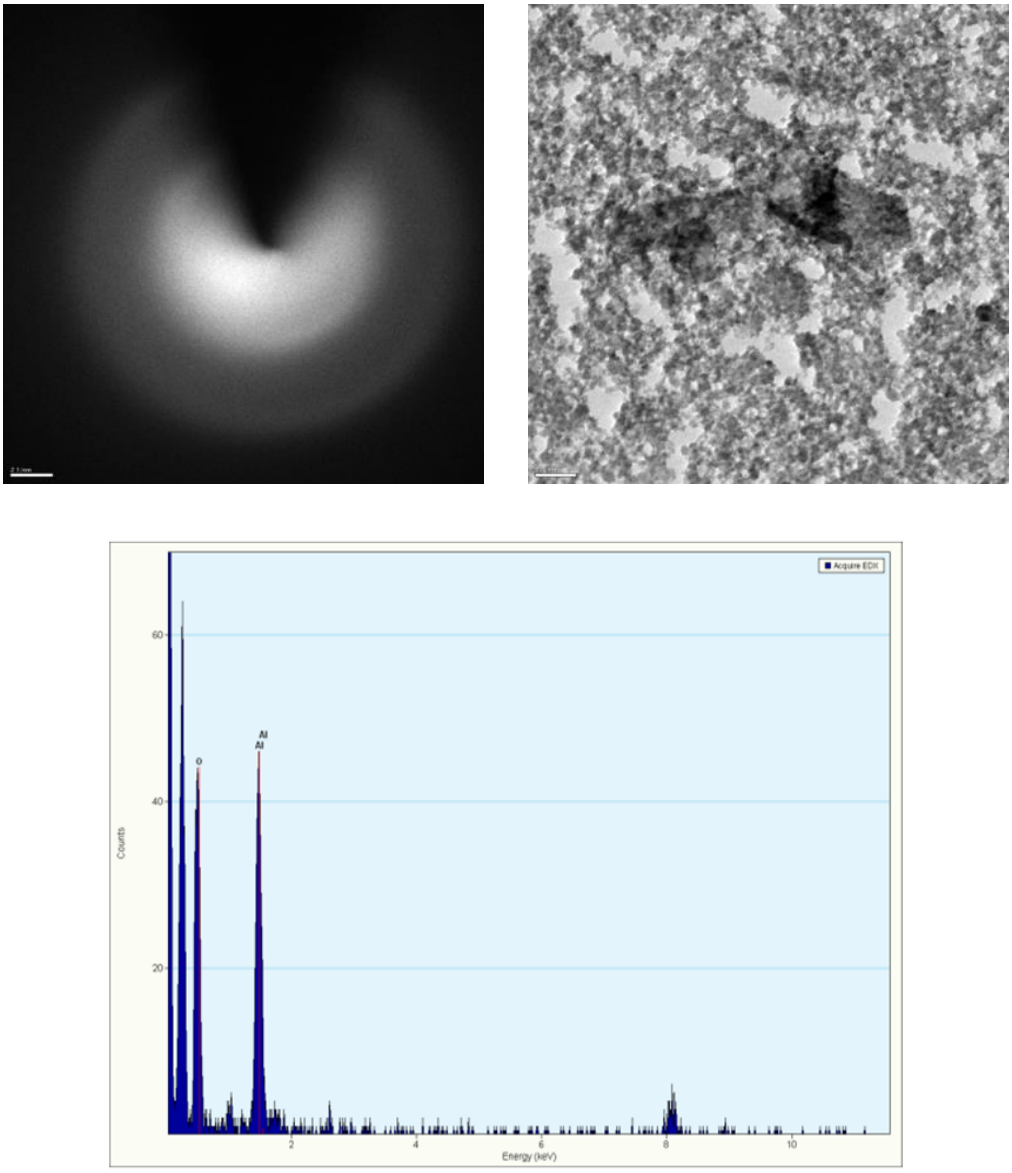

Figure 52 - TEM analysis (IC sample (area 3) for pH 8.2 test).

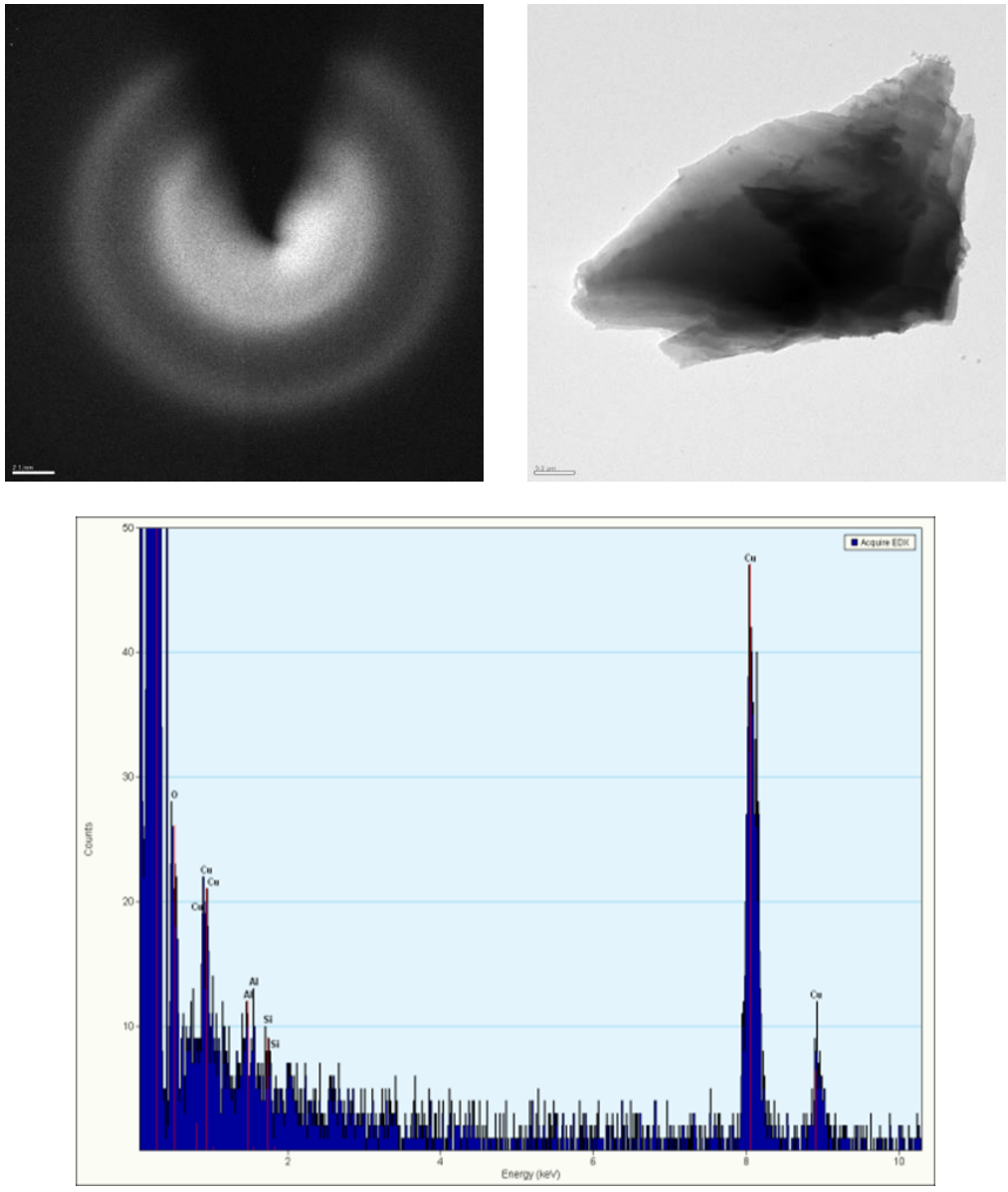

Figure 53 - TEM analysis (SC sample (area 3) for pH 8.2 test).

It should be remarked that, due to the low concentration of Al in the samples analyzed, statistical analysis was not conducted for this test. In particular, particles shown in the Figure 51 and Figure 53 were isolated when performing the scanning and information on the presence of similar particles in the sample analyzed is not reported. Figure 52 shows the TEM results for the IC sample. The analyses confirmed that the presence of boron did not affect the measurements since concentrations of boron in the areas analyzed were almost undetectable. It has also to be remarked that the intensity peak of the oxygen may be affected by the inevitable presence of this element in atmospheric composition.

DISCUSSION

It should be noted that the higher pH corrosion tests resulted in higher solution turbidity in general. This is expected as the dissolved ion concentration is higher due to the increased solubility limit in this environment. The RC samples of the corrosion tests resulted in discreet particle sizes rather than multiple particle sizes as seen with the slower cooled and surrogate samples.

The cooling rates were held as constant as possible during testing. Some inconsistencies in the cooling rates which can most noticeably be seen in Figure 10 and Figure 12 were the result of a disturbed thermocouple while the test was in progress. The three cooling rates selected for each test were not identical in their cooling rate parameters. The slow cooled samples were placed into an oven which provided a slower total cooling time, but introduced a step-down cooling rate. This resulted in a plateau in the temperature around 50-60 ℃ before the oven was turned off to finish the cooling process. The cooling rates were calculated as a linear average cooling rate using Equation 1 below.

$$C_R = \frac{(\mathrm{Ti} - \mathrm{Tf})}{t_t} \qquad \text{Equation 1}$$

Where:

C_R = Cooling Rate
T_i = Initial Temperature
T_f = Final Temperature (25 °C)
t_t = Total Cooling Time

The final temperature was set for each test with a T_f of 25 °C. The effects of this step-down cooling process in the slow cooled samples were assumed to be minimal in comparison to a natural cooling rate, but should be further explored to confirm this assumption.

Selected samples were monitored for turbidity over time as a method to indirectly monitor particle size. The solution turbidity is a function of both particle size and quantity. Although there was no substantial change over time recorded for turbidity measurements for any of the tests, not all samples were guaranteed to have no change in particle size. Only selected samples were tested due to prohibitive cost of analysis. A trend was observed showing the sample turbidity as an increasing function of cooling time for the three pH tests that were conducted.

The particle size for all tests had a strong correlation with cooling rate. The large variation in the particle size for the RC samples in all pH tests is likely due to the variation in cooling rate due to the relative position in the ice bath. Although the samples were agitated periodically, there was unavoidable temperature stratification in the

sample containers while they were cooled. This resulted in multiple cooling rates within a given RC sample.

The method of particle size analysis was based on the DLS method using the Brownian motion of the particles which causes the incident laser light to be scattered at various intensities. This method works well for particles that are symmetric and round with a polydispersity index (PDI) close to 1. However, with some of the larger particles that were measured, there was a substantial uncertainty that was introduced due to a low PDI.

EDS cannot detect hydrogen so the exact compositional information cannot be confirmed. However, since the ratio of Al to O is 0.5 for AlOOH and 0.67 for Al_2O_3, it may be plausible to assume that the RC sample may have produced AlOOH compounds. Slower cooling rates may have produced two different Al compounds, namely AlOOH (both in amorphous or crystalline structure) and Al_2O_3.

The 3103/3203 and 3103R/3203R test series has some discrepancies in the reproducibility of the data. The repeat test was run to confirm the unexpected turbidity results where the increased cooling rate did not produce a consistently higher turbidity measurement in the intermediate sample. The inconsistency in the turbidity results did not reflect an oddity in the particle size however as the trend was the same as the other two tests that were performed. The test was repeated regardless to see if this result was from a possible error in testing or equipment response. The 3103R/3203R test did result in a turbidity trend that was as originally expected and similar to the other tests. The

particle sizes were however much smaller than expected based on results from the previous 3103/3203 test. It was noted during testing when at test termination, a foil roll was observed to have been transported to the pump intake (V-C1-1). This resulted in a decreased solution flow rate across the aluminum sample likely causing a lower concentration of dissolved ions than expected at test termination. This was confirmed during the ICP-MS analysis when the dissolved aluminum concentration was determined to be about half of that from the original 3103/3203 test result. The sample from the original 3103/3203 test that was decanted and dried was sent for XRD analysis, but unfortunately no aluminum was found in the sample. This proposes the hypothesis that the aluminum particles generated were still suspended in the decanted solution that was discarded while preparing the solid sample for XRD analysis. The drying process also can impact the structure of the precipitate formed under certain circumstances (Klasky 2006).

It was not originally expected that the particle size would be heavily dependent on the final concentration of the solution for similar pH test runs. This unexpected result from the 3103R/3203R test could lead to additional tests being performed in this area to confirm the particle behavior as a function of aluminum concentration.

SUMMARY AND CONCLUSIONS

The test facility at Texas A&M was used to generate post-LOCA precipitates. An initial bench scale corrosion analysis provided information necessary on scaling up the experiment. The process was scaled to a 190L tank and the effects of pH and temperature on concentration, turbidity and morphology of the particles generated was analyzed. It was found that pH had a significant effect on the concentration of aluminum in solution as well as the number of particles generated. An increase in pH subsequently increased the concentration of precipitates generated. The cooling rate also affected the size of the particles and the crystallinity of the precipitates. Overall, an increase in the total cooling time increased the size of the particles generated. The rapid cooling rate produced AlOOH as the precipitate which was determined from the EDS analysis. These particles were generally non-homogeneous in nature. The generation of aluminum precipitates from the $Al(NO_3)_3 \bullet 9H_2O$ resulted in particles that are a suitable substitute for additional head loss testing in the GSI-191 project.

The intermediate cooling rate produced particles that were more uniform in size and also tended to form other morphological forms of Al_2O_3 apart from Υ-alumina, sometimes forming AlOOH as well. Slow cooling also generated homogenous amorphous particles with an O to Al ratio of around 4 indicating the possible formation of boehmite or diaspore compounds. Characterizing these particles can add to the database of effects of pH and temperature on alumina as well as help in creating new

surrogates for testing the effects of these particles on the strainers for large scale head loss testing.

FUTURE WORK

Characterizing these particles will help in creation of surrogate salts that have similar morphology as actual corrosion products, and thus can be used for larger scale head loss testing. The surrogates can also be considered as representative post-LOCA particles validating existing tests and allowing for simplification of additional tests. This can help in the design of more accurate head loss testing models. Further work also involves testing the presence of other metals on the concentration and morphology of alumina precipitates as well as the impact of ion concentration as well as pH. A correlation between turbidity and concentration and particle size can also be established for easier analysis and characterization using turbidity data alone.

REFERENCES

Ali, A., et al. (2016). "Corrosion and solubility in a TSP-buffered chemical environment following a loss of coolant accident: Part 4 – Integrated chemical effects testing." Nuclear Engineering and Design 300: 644-654.

Bahn, C. B. (2013). "Chemical Effects on PWR Sump Strainer Blockage after a Loss-of-Coolant Accident: Review on US Research Efforts." Nuclear Engineering and Technology 45(3): 295-310.

Bahn, C. B., et al. (2009). "Evaluation of precipitates used in strainer head loss testing. Part I. Chemically generated precipitates." Nuclear Engineering and Design 239(12): 2981-2991.

Borchardt, R. W. (2012). Closure Options for Generic Safety Issue - 191, Assessment of Debris Accumulation on Pressurized-Water Reactor Sump Performance, Document No. SECY-12-0093, US Nuclear Regulatory Commission, Washington, DC

Fullerton, C. (2015) (1). "Analysis of Aluminum Precipitate for 3000 Series Test – Test 3101 - 3201. Unpublished

Fullerton, C. (2015) (2). "Analysis of Aluminum Precipitate for Test 3000 Series – Test 3102 - 3202. Unpublished

Fullerton, C. (2015) (3). "Analysis of Aluminum Precipitate for Test 3000 Series – Test 3103 – 3203. Unpublished

Fullerton, C. (2015) (4). "Analysis of WCAP Precipitate for Test 1100." Unpublished

Ghosh, A. K., et al. (2007). "Head loss characteristics of a fibrous bed in a PWR chemical environment." Nuclear Technology 157(2): 196-207.

Institute, N. E. (2004). "NEI 04-07 - Pressurized Water Reactor Sump Performance Evaluation Methodology."

M. Klasky, J. Z., M. Ding, B. Letellier (2006). "Aluminum Chemistry in a Prototypical Post-Loss-of-Coolant, Pressurized-Water-Reactor-Containment Environment." United States Nuclear Regulatory Commission NUREG/CR-6915(LA-UR-05-4881): 1-80.

Lahti, E., et al. (2014). "Material corrosion in a reactor containment sump following a loss-of-coolant accident." Progress in Nuclear Energy 75: 1-9.

Leavitt, J. J., & Fullerton, C. (2013). Unpublished aluminum and silicon NMR results. University of New Mexico, Albuquerque, NM.

A.E. Lane, T.S. Andreychek, W.A. Byers, R.J. Jacko, E.J. Lahoda, E.J. Lahoda, R.D. Reid"Evaluation of Post-Accident Chemical Effects in Containment Sump Fluids to Support GSI-191," WCAP-16530-NP-A, Westinghouse Electric Company (2008)U.S. NRC ADAMS Accession No. ML081150379.

Lee, J.-I., et al. (2011). "Evaluation of recirculation sump performance for OPR1000 plant: Part I debris transport during the blow-down phase of LOCA." Annals of Nuclear Energy 38(2–3): 681-693.

Leeds, E. (2010). "Reconsideration of General Design Criterion 4 (GDC-4) Application to Generic Safety Issue (GSI) 191." NEI M(ML101050354).

Regulation, U. S. N. R. C. O. O. N. R. (1996). "NRCB 93-02 – Debris Plugging of Emergency Core Cooling Suction Strainers." NRC Bulletin 93-02.

Regulation, U. S. N. R. C. O. O. N. R. (1996). "NRCB 96-03 - Potential Plugging of Emergency Core Cooling Suction Strainers by Debris in Boiling-Water Reactors." NRC Bulletin 96-03.

Sandrine, R., et al. (2008). "Precipitate formation contributing to sump screens clogging of a nuclear power plant during an accident." Chemical Engineering Research and Design 86(6): 633-639.

Vujičić, V. and B. Lovreček (1985). "A Study of the influence of pH on the corrosion rate of aluminium." Surface Technology 25(1): 49-57.

Zhou, Q., Zhao, H. L., Shao, Z. C. et al. (2012). Influence of Parameters on Alumina Particles Size and Morphology. In Advanced Materials Research (Vol. 382, pp. 336-339). Trans Tech Publications.